COMPUTATIONAL FLUID DYNAMICS (CFD) ANALYSIS OF LATENT HEAT STORAGE IN HEAT EXCHANGERS BY USING PHASE CHANGE MATERIALS (PCM)

A Thesis Submitted to
the Graduate School of
İzmir Institute of Technology
in Partial Fulfillment of the Requirements for the Degree of

MASTER OF SCIENCE

in Energy Engineering

by
İsmail Gürkan DEMİRKIRAN

July 2020
İZMİR

ACKNOWLEDGMENTS

Firstly, my gratitudes are to my advisor Assoc. Prof. Dr. Erdal ÇETKİN for his inspiring scientific point of view and continuous motivation throughout my researches. I would like to thank my co-advisor Prof. Dr. Luiz A. O. ROCHA who supported my studies with his kindness even in pandemic days.

I would like to thank to Zeynep KAHRAMAN who taught me to be patient and zealous and to Ezgi ŞATIROĞLU for her valuable support at harsh times of my study.

Finally, my special thanks are to my mother Hüsne DEMİRKIRAN, my grandmother and grandfather Sevim DEMİRKIRAN and Hasan DEMİRKIRAN for their endless supports and self-sacrifices until now.

ABSTRACT

COMPUTATIONAL FLUID DYNAMICS (CFD) ANALYSIS OF LATENT HEAT STORAGE IN HEAT EXCHANGERS BY USING PHASE CHANGE MATERIALS (PCM)

The development of TES applications and materials takes the attention of many researchers, but the current literature rarely involves studies concerning medium temperature applications. This thesis compares available phase change materials (PCMs) for the medium temperature range. For this aim, Erythritol was defined as PCM in the numerical analyses. The effect of heat transfer fluid (HTF) tube position and shell shape on the melting time and sensible energy requirement for melting a phase change material (PCM) in a latent heat thermal energy storage (LHTES) application were investigated. Tube location and shell shape are essential due to the shape of the melted region, i.e., similar to the boundary layer. Results show that the S-curve of melting becomes steeper if the tubes are distributed such that the intersection of melted regions is delayed. Therefore, melted regions should be packed into a finite space which uncovers the shape of the shell that minimizes melting time and required sensible energy. Results show that, rectangular-shaped shell design where the tubes located near the bottom end decreases melting time and sensible energy from 67 minutes to 32 minutes and from 161.8 kJ/kg to 136.3 kJ/kg for %72.3 liquid fraction relative to the circular-shaped shell, respectively. In the four-tube cases, then the required melting time and sensible energy decrease 80% and 3.8% through the rectangular-shaped shell design for the PCM to melt completely, respectively. Overall, the results show that sensible energy storage and especially melting time can be decreased greatly by just varying the design.

Keywords**:** *Phase Change Material; Thermal Energy Storage; Design Optimization; Shell and Tube Heat Exchanger; S-curve*

ÖZET

FAZ DEĞİŞTİREN MALZEMELER KULLANILARAK ISI DEĞİŞTİRGEÇLERİNDE GİZLİ ISI DEPOLAMANIN HESAPLAMALI AKIŞKANLAR DİNAMİĞİ ANALİZİ

TED uygulamalarının ve malzemelerinin geliştirilmesi birçok araştırmacının dikkatini çekmektedir, ancak mevcut literatür nadiren orta sıcaklık uygulamaları ile ilgili çalışmaları içermektedir. Bu tez, orta sıcaklık aralığı için uygun faz değişim malzemelerini (FDM) karşılaştırmaktadır. Bu amaçla, sayısal analizlerde FDM olarak Erythritol tanımlanmıştır. Gizli ısı termal enerji depolama (GITED) uygulamasında, bir faz değiştiren malzemenin (FDM) eritilmesi için ısı transfer akışkan (ITA) tüpünün konumu ve kabuk şeklinin erime süresi ve duyulur enerji gereksinimi üzerindeki etkisi incelenmiştir. Tüp konumu ve kabuk şekli, erimiş bölgenin şeklinin sınır tabakaya benzer olması nedeniyle önem arz etmektedir. Sonuçlar, FDM erimiş bölgelerin kesişimi gecikecek şekilde paylaştırılırsa erimenin S-şekilli eğrisinin daha dik hale geldiğini göstermektedir. Bu nedenle, erimiş bölgeler, erime süresini ve gereken duyulur enerjiyi en aza indiren kabuk şeklinin oluştuğu sonlu bir alana sığdırılmalıdır. Sonuçlar, tüplerin alt sınıra yakın konumlandırıldığı dikdörtgen şekilli kabuk tasarımının dairesel şekilli kabuğa kıyasla 72.3% erime oranı için erime süresini ve duyulur enerjiyi sırasıyla 67 dakikadan 32 dakikaya ve 161.8 kJ/kg' dan 136.3 kJ/kg' a düşürdüğünü göstermektedir. Dört tüplü durumlarda ise, FDM’ nin tamamen erimesi için dikdörtgen şekilli kabuk tasarımı sayesinde gerekli erime süresi ve duyulur enerji sırasıyla 80% ve 3.8% azalmaktadır. Genel olarak, sonuçlar duyulur enerji depolamanın ve özellikle erime süresinin sadece tasarımı değiştirerek büyük ölçüde azaltılabileceğini göstermektedir.

Anahtar Kelimeler ve Deyimler: *Faz Değiştiren Malzeme, Termal Isı Depolama, Tasarım Optimizasyonu, Kabuk ve Borulu Isı Değiştirgeci, S-eğrisi*

TABLE OF CONTENTS

LIST OF FIGURES

Figure **Page**

LIST OF TABLES

LIST OF SYMBOLS

A	Porosity function	$kg/(m^3.s)$
b	Dummy constant	
c_p	Specific heat	kJ/(kg.K)
C	Mushy zone constant	$kg/(m^3.s)$
f	Liquid Fraction	
g	Gravitational acceleration	m/s^2
h	Enthalpy	kJ/kg
k	Thermal conductivity	W/(m.K)
L	Latent heat capacity	kJ/kg
P	Pressure	Pa
q	Heat flux	W/m^2
S_b	Buoyancy source term	$kg/(m^2.s^2)$
S_h	Energy source term	W/m^3
t	Time	s
T	Temperature	°C
u, v	Velocity components	m/s
x, y	Spatial coordinates	m

Greek Letters

μ	Dynamic viscosity	kg/(m.s)
ρ	Density	kg/m^3
β	Thermal expansion coefficient	1/K

Subscripts

amb	Ambient
f	Final
i	Initial
l	Latent
liquidius	Liquification point
m	Melting
ref	Reference
t	Thermal
s	Sensible
solidius	Solidification point

CHAPTER 1

INTRODUCTION

When looked at the history of human beings, energy has been one of the basic physiological needs of people like nutrition, sheltering, sleeping even if it does not directly figure in the Maslow's hierarchy. While the primitive man needed energy only for warming or cooking, energy has been used for the manufacturing of pottery and swords in time. The industrial revolution and invention of electricity added a new dimension to the human-energy relation. People have started to produce more and more, and energy need has showed an incredible increase. In the last century, the world population has quadrupled. Today, the population has exceeded 7.5 billion, and the projections show that it will come close to 9.7 billion by 2050. This increase in the population and technological developments lead increase in energy consumption to continue. At present, the consumption is six times higher than in the past century(Ritchie and Roser 2018). These energy consumption amounts express how developed the societies are. However, it also explains why all living creatures suffer from the greenhouse emissions, because demanded energy is supplied from the fossil sources such as coal, petroleum, natural gas. Increasing emissions cause people to get cancer, heart, and respiration diseases, and are responsible for the extinction of many plant and animal species. In recent years, the negative impact of CO_2 emissions on global climate change has begun to be perceivable much more. This situation has led the governments to renewable energy systems, and establish new energy policy and strategies to subsidize zero-carbon-foot-print energy technologies. Carbon taxes and emission penalties are at issue for the governments and companies, not fulfilling the requirements towards the KYOTO protocol. In the history of the energy sector, the 1973 year is a breaking point, when the Organization of the Petroleum Exporting Countries (OPEC) put an embargo on crude oil prices, and especially European countries were being destitute of their main energy source. For this reason, the governments have attempted to find new energy sources alternative to fossil fuels("1973 Oil Crisis - Wikipedia" n.d.). However, it seems that renewables are back-marker in the energy competition, although it is the most environment-friendly solution. And unfortunately, current investments on renewable

energy technology are still not enough to reduce energy-related emissions. According to 2018 statistics of International Energy Agency (IEA), only 26% of electricity production is by renewables. The remained part is still supplied by coal, gas and nuclear with the share of 38%, 20% and 10%, respectively. The projections reveal that global energy needs will increase by 1.1% yearly until 2040(IEA 2019). There is an important question: How long will the world be able to resist?

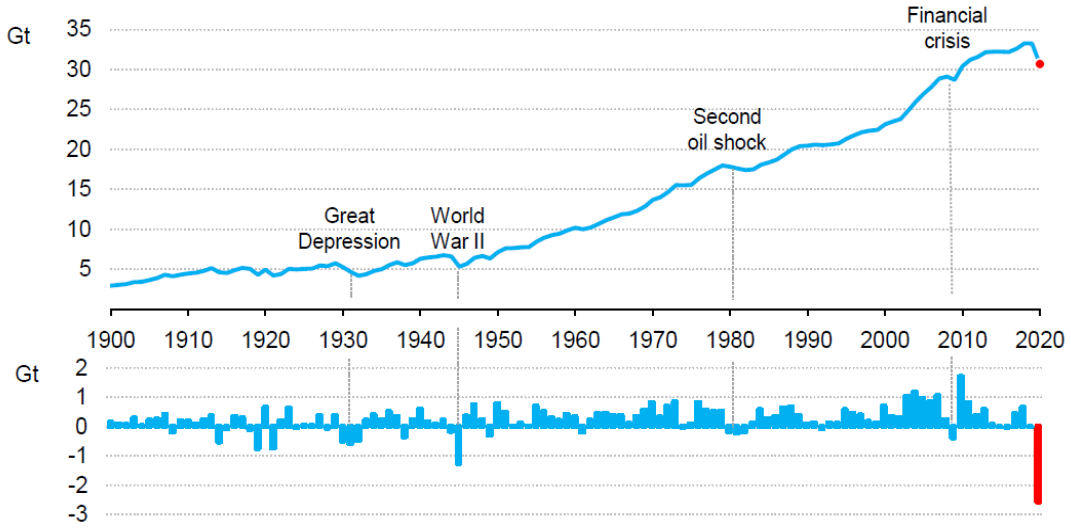

Figure 1.1. The decrease in energy-related CO_2 emissions between the years of 1900-2020 (Source: (IEA 2020))

The desired decrease in greenhouse emissions occurred due to unprecedented coronavirus pandemic, not by renewables. Such a fluctuation in emissions has never seen before in history, as demonstrated in Fig. 1.1. As the biggest responsible of the emissions, in China with coal-powered industry, the satellite image in Fig.1.2 confirms the decrease of the NO_2 levels. The Chinese New Year corresponds to the time of the virus's appearance. Daily data analysis of IEA at the mid-April demonstrates that fall in energy demands are 25% and 18% averagely in full lockdown and partial lockdown of countries, respectively. The expectation in the decline of global CO_2 emissions is by 8% compared to the previous year (IEA 2020). The world has experienced this sharp decrease because the industry stopped the production activities. In addition, people were in less roaming worldwide during the lockdown, so automobile emissions dropped due to efficient fuel

combustion in the lack of heavy city traffic. China is one of the first countries that began industrial production back after the COVID-19. China will likely face depression in the export of oversea commercial products. Production will similarly decrease for the rest of the world, too. However, energy demand will rebound to the levels before the crisis in time. Therefore, investments on low carbon renewable energy technologies are crucial not to bring the emissions back. Moreover, renewable energy is a resilient choice to surpass the bad effects of the crisis stemming from the COVID-19 due to its accessibility to various power systems.

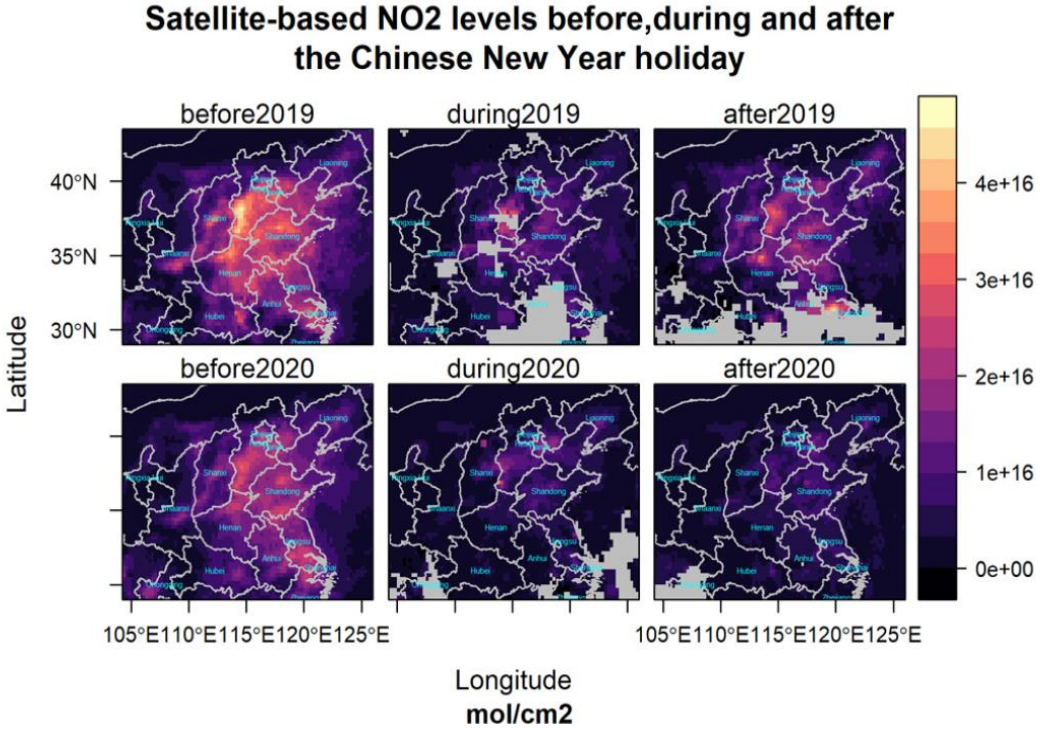

Figure 1.2. NO_2 concentration before and after the COVID-19 crisis in China (Source:("Analysis: Coronavirus Temporarily Reduced China's CO2 Emissions by a Quarter" n.d.))

IEA-World Energy Outlook 2019 reports that shares of renewables in electricity generation are 61.5% for hydro, 19.2% for solar, 7.7% for wind, and 11.5% for the others(IEA 2019). Due to sharp reductions in costs, and policy supports, particularly solar and wind have grown in recent years. The important issue for any energy generation system is to be cost-competitive or not. Capacity factor of the system has a significant

impact on energy efficiency. On the other side, it is expected from the system to be financially convenient and sustainable. Using the levelized cost of energy (LCOE) is a good way to compare different energy generation plants. It is calculated as the overall costs of the system divided by produced energy during the life-time span. Figure 1.3 shows that solar PV and wind technologies are more energy-economic with lower LCOE levels compared to conventional energy production methods (coal-fired or gas combined cycles). With tax subsidizations, it can get to a much lower extent. Therefore, solar PV and wind technologies can be preferred rather than conventional generation plants.

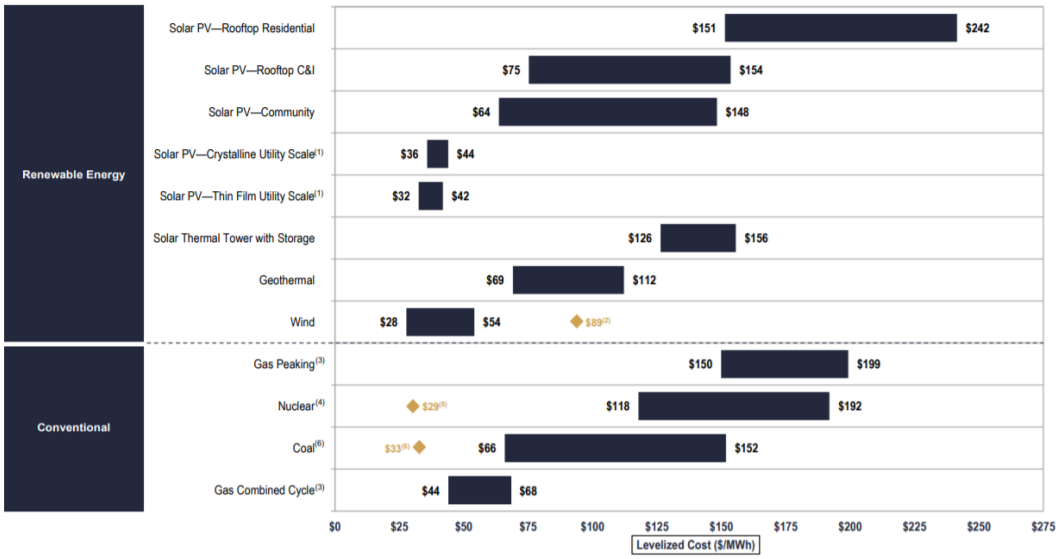

Figure 1.3. LCOE comparison of renewable and conventional energy systems without government subsidizations (Source:(“Lazard.Com | Levelized Cost of Energy and Levelized Cost of Storage 2018” n.d.))

Governments ask the bidding strategy (if not applied tariff-model) from the operators of energy generation plants. The bidding assures of energy production amount, price, and the time when the electricity network will be fed and is important for the liberalized day-ahead market and energy supply-demand. To determine these parameters is relatively easy for conventional energy producers, there is no disruption as long as a fuel crisis on the supply chain does not occur like the 1973-74 OPEC crude oil embargo. On the side of renewable energy producers, there is a strong dependence on natural circumstances. Wind, rain, solar radiation show variances according to the movement of

the earth around the sun and itself. This situation causes daily, weekly or monthly fluctuations on the predictions of the parameters such as temperature, humidity, wind direction, and wind flow magnitudes. Moreover, increasing global warming continues to change regional climate regimes, and makes it gradually difficult to predict weather conditions in low error. One of the best options that will be able to save renewable energy producers from intermittency of nature is energy storage. Energy storage is to extend the operation time to the whole day. When the energy storage unit is adopted in a concentrated solar power (CSP) plant, the generation will be carried out during also night-time duration so that the system will be operating as if it is a fossil-fuel-driven Rankine cycle. Instead, it is possible to store surplus energy since the demand decreases and is low-priced at night-time operation. Thus, the energy can be discharged high priced in the day-time.

Figure 1.4. Change in the LCOE amounts of CSP plants commissioned between 2010 to 2018 (Source:(IRENA International Renewable Energy Agency 2018))

When mentioned about ‘energy storage’, the first thing that comes into mind is rather the storing of electricity. It can be stored via electrochemical batteries or supercapacitors, and has a vital role in transportation, electronic devices, power network management and energy systems efficiency. On the other hand, there are many storage types of various energy forms such as chemical, mechanical or thermal energy storage, etc. Among them, thermal energy storage (TES) is also on the focus of interests for scientists. Heat energy occupies 50% of the total energy consumption and is guilty of 40% CO_2 emissions in the world. While nearly one half of the produced heat is used for heating, cooling, and hot water need of buildings, the other half is used in industrial processes. Modern renewables (excluding traditional use of biomass, e.g., burning of wood) has met only 10% of global heat demand in 2018(“Heat – Renewables 2019 – Analysis - IEA” n.d.). Thermal energy technologies should be improved to close the gap between heat energy demand and supply by renewables. At this point, the LCOE evolution of CSP plants is a good example to comprehend the crucial act of TES. Due to being cheaper of installation and improvement in the capacity factors in recent years, the LCOE of CSP become 0.0185 $/kWh in average, which is 40% lower than the price of 2010(IRENA International Renewable Energy Agency 2018). Figure 1.4 obviously reveals the reduction in the LCOE due to the addition of the storage unit and an increase in storage hours. There are no commissioned CSP projects without storage units since 2014.

It can be made a list of utilization areas to integrate TES units. Solar trough power plants are the most convenient fields of TES to balance the demand-supply relation and to make electricity generation possible during the night-time(Vaivudh, Rakwichian, and Chindaruksa 2008). In addition to power generation by solar energy, these solar thermal plants with TES units can provide industrial process steam in the absence of solar radiation. ORC-powered solar thermal plants integrated with TES is a good candidate to get the thermal energy responsibility of small rural settlements (~200kW_t) (Lakhani, Raul, and Saha 2017), and to provide daily domestic needs(Gorzin et al. 2018). Apart from the renewable energy plants, an alternative utilization field of TES is the waste heat recovery. TES integrated catalytic convertor can be given as a good example of cold start mechanism(Kato et al. 2009). Besides CO_2 emissions, NO_x and SO_x released from the vehicles, threatens human health. Although European countries began to ban diesel engines, it seems that most of the world will continue to use fuel-powered cars in the

upcoming years. Therefore, governments promote people to buy hybrid cars. In hybrid cars, the electric battery is charged kinetically by converting excess work to electricity. The stored electricity helps the combustion engine to work less and in a more efficient way. Also, the integration of a thermal battery into the hybrid system benefits the reduction of emissions. Thermal battery, charged by exhaust gas of the engine, keeps the temperature of catalytic convertor at 200-300°C that is the optimum working interval. Moreover, industry (especially food, brewery, and chemical industries) meets with TES in the need for thermal management of waste heat(Achkari and El Fadar 2020). Since the integration of TES provides an increase in energy-saving, excess energy need and emissions fall. TES does a good job also at removing or decreasing the thermal load of the building and at establishing thermal comfort.

CHAPTER 2

THERMAL ENERGY STORAGE (TES) TECHNIQUES

There are three thermal energy storage types in use and being presently under investigation. These are sensible heat storage, thermochemical heat storage, and latent heat storage.

2.1. Sensible Heat Storage (SHS)

The first type, sensible heat storage (SHS), works with the principle of raising and falling of the temperature within the limits of substances' specific heat capacity. Equation 2.1 explains how to calculate the storage capacity of sensible heat storage medium as below:

$$q = \int_{T_i}^{T_f} m \, c_p \, dT \tag{2.1}$$

where m is the mass of the storage medium, c_p is the specific heat. T_i and T_f represent the initial and final temperatures of the medium, respectively. Sensible heat can be stored in solid materials such as rocks, concrete which are easy-producible, abundant and cheap. Solid storage medium needs long pipes that serve for heat release and extraction. Moreover, it requires huge tank volumes to store excess heat, but also heat transfer fluids in large amounts. Recently becoming a popular method for SHS, especially for solar applications, is to store heat in a liquid medium. Fluids, such as thermic oils or molten salts selected by concerning working temperature, are applied not only as heat transporter but also heat storage medium. The so-called thermocline system involves only one storage tank which accommodates hot and cold fluid separately by thermal stratification. Thereby, the thermocline system is financially more feasible, because it is not necessary

to invest an extra storage tank and heat exchangers. But SHS falls behind other storage techniques, regarding ascending future energy demand. The energy density of SHS materials is much lower relative to latent heat storage capability. Also, the thermal conductivities are in the range of 0.2 to 2 W/mK, which concludes SHS is not superior in terms of charge/discharge rates(Achkari and El Fadar 2020). Besides, molten salts and other fluids have high solidification points, and hence, there is a risk of solidification in thermocline storage tanks due to thermal losses.

2.2. Thermochemical Heat Storage (THS)

Thermochemical heat storage (THS) has the least academic maturity among TES types. It based on the principle of conversion of reactants and products to the other by reversible thermochemical reactions. Thermal energy is stored/released by endothermic/exothermic reactions. Thermochemical storage has two prominent features. The first is, enthalpy of reaction promises to store considerably more thermal energy than sensible heat storage (by specific heat) and latent heat storage (by fusion enthalpy). Hence, it provides the same amount of energy at a lower volume tank. The latter is that there is no need to thermally insulate the storage tanks because thermal energy acts on the forming and destroying of chemical bonds and no losses exist. These two features make investment and operation cost levels down. On the other side, reactants and products must be heated to start the reaction and to constitute an environment for catalysts that increases reaction rate during charging and discharging. This is the adverse aspect of THS in terms of costs.

$$NH_3 + \Delta H \longleftrightarrow \frac{1}{2} N_2 + \frac{3}{2} H_2 \ \Delta H = 66.5 \text{ kJ/mol} \tag{2.2}$$

$$CH_4 + H_2O + \Delta H \longleftrightarrow 3H_2 + CO \ \Delta H = 206.2 \text{ kJ/mol} \tag{2.3}$$

As a widely used material in the industry, dissociation of ammonia (2.2) is a good example of THS, that works at ambient temperature (T_{amb}=25°C). There occurs no side reaction during the process since ammonia condenses at ambient temperature. However, the reaction enthalpy of disassociation of ammonia is relatively low, ΔH=66.5 kJ/mol. Another reaction, which operates at ambient temperature (T_{amb}=25°C), is steam reforming of methane (2.3) that is an example of catalytic reactions. With reaction enthalpy of ΔH=206.2 kJ/mol, this reaction is superior to the previous one.

This method will become an up-and-coming technology. However, it is at laboratory scale today, and still needs further improvements on topics of safety (toxicity, flammability), reversibility, and reaction rates to reach commercially producible.

2.3. Latent Heat Storage (LHS)

Latent heat storage (LHS) is based on the phase transition of materials. This transition is from solid to solid, solid to liquid or liquid to gas with so-called phase change materials (PCM). In the solid-solid phase transition, crystalline form of solid changes from one to the other. $NaNO_3$ undergoes solid-solid phase change at 214°C or water has seven different solid phase at different temperatures, but a considerable enthalpy change and volume change are not observed(Carrasco Portaspana 2011). The highest enthalpy change is observed in the liquid-vapor phase transition (evaporation and condensation). But since volumetric expansion is too high after evaporation the liquid-vapor option is impractical. Also, storage tanks should be resistive enough to high pressure after evaporation. So the most feasible LHS method is the solid-liquid phase transition.

PCM stores heat in latent form while it melts, it releases heat while it solidifies, where the processes correspond to charging and discharging of storage systems, respectively. One advantage of LHS is that heat of fusion has a greater storage potential in comparison with specific heat for unit volume. The other is that phase change occurs at isothermal or nearly isothermal conditions which provides to extract heat from the system at constant temperature. Figure 2.1 reveals the temperature-enthalpy relationship over isothermal melting and solidification processes. The PCM temperature increases until the melting point, sensible heat enthalpy increases at the same time. With the start of the melting process, the temperature is fixed to a constant value, but an incredible enthalpy increase happens in latent form. After finishing the melting, the temperature

continues to increase if the heating goes on too. On the other side, among thermal energy storage types, the most detrimental one for the environment is LHS since high emissions released during system manufacturing and material production.

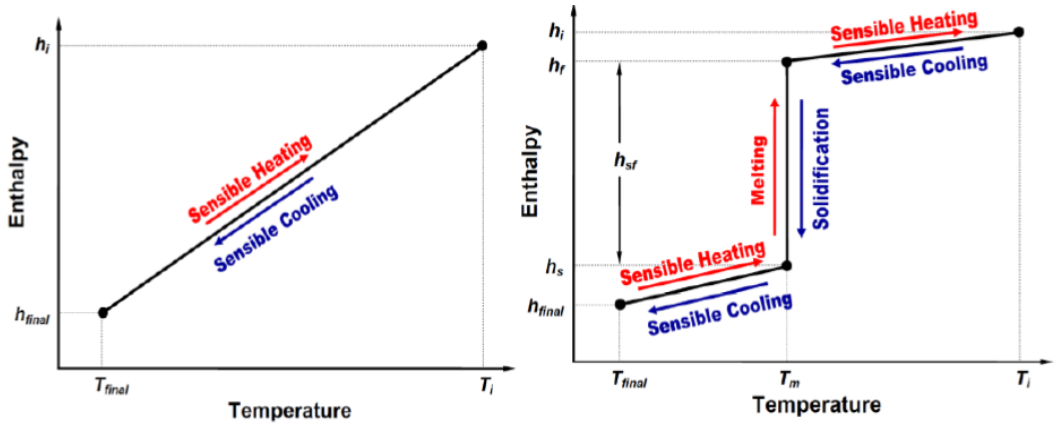

Figure 2.1. Temperature-enthalpy relationship during latent heat storage, sensible heating and cooling of PCM (Source:(Ezan, Ozdogan, and Erek 2011))

CSP plants can serve the industry which needs steam at 128 bar and 400°C along the day time and night time (with the integration of TES). CSP plants commissioned ever powered by SHS units, but this hybrid system, called direct steam generation, applies SHS and LHS units together. Despite seen rarely in literature, a latent heat thermal energy storage (LHTES) unit at a huge scale energy system was tested by Laing et al(D Laing, T Bauer, W.D Steinmann 2009). The test facility has run for 4000 hours and 172 cycles with 140kg PCM ($NaNO_3$), which showed repeatability and no corrosion. Then, a real-scale storage unit was constructed including 14tons of PCM with 680 kWh heat storage potential(Laing et al. 2011a). The system discharges the stored energy by SHS units, which is responsible for preheating and superheating of the steam, and by LHS units, which evaporates water within phase change materials, and supplies steam for industry. While the concrete storage system supplies 30% of thermal energy needs, the PCM storage does 70%. The plant was installed in Carbonera, Spain.

CHAPTER 3

BASICS OF PHASE CHANGE MATERIAL (PCM)

The role of PCM, being used as storage material in TES applications, has mentioned in the previous chapters. Out of energy storage mission, PCM has alternative utilization fields such as thermal management of PV panels, passive cooling of electronic equipment and batteries, drug and food delivery devices(Celik et al. 2019; Al-Abidi et al. 2013). In PV panels, temperature values that exceed the critical degree decrease energy conversion efficiency. In addition, the utilization of PCM in the PVT system contributes to obtaining domestic hot water. Similarly, the temperatures higher than 80°C may damage computer processors.

The selection of PCM and to determine proper working conditions is an important issue for any application. The selected PCM has to fulfill physical, chemical, thermal, and financial requirements. The melting temperature of PCM should fit the operating temperature range of the application, and it is desired to have high fusion enthalpy and thermal conductivity. Phase segregation, supercooling, chemical, and thermal instability induce phase change to get difficult or even be able to stop.

Adequate crystallization rate is essential at preventing supercooling. During the solidification process, HTF circulates at the temperature lower than the melting temperature of the PCMs. It is expected melted PCM to convert to solid, but solidification does not begin although the temperature falls below the melting point. The reason why this situation, called supercooling, occurs is that the crystallization growth rate of the particles is not as much as the solidification rate. This situation continues with the temperature rising to the solidification point of PCM again and resulted in delay in the discharging process and non-uniform heat transfer(Agyenim, Eames, and Smyth 2010). Many factors cause supercooling, including the degree of purity, the occurrence of bubble nucleating, and boundary conditions. To overcome the bad effects of supercooling, composite PCMs doped with nucleating agents can be used. Some of them (e.g. CaPi, TMB-5) reveals stability during melting-crystallization processes. However, they cause a decrease in latent storage capacity and phase change transitions occur at lower temperatures than the melting temperature of the pure PCM. Another solution to prevent

supercooling is being dispersed of nanoparticles inside PCM. In addition to enhance the overall thermal conductivity of PCM, nanoparticles continue to retain their crystal forms after the melting of PCM and have a function of nucleation(Zeng et al. 2017).

Another important point is the compatibility between PCM and container material. The density of PCM, especially after it melted, exhibit falling tendency while temperature increases, and it concludes with volumetric thermal expansion of PCM. The volumetric expansion may cause thermal stress and leakage problems. Also, corrosion causes leakage of melted PCM in long term period and maintenance problems. Leakage of PCM engendered termination of operations at the DLR test facility in 2007(Laing et al. 2011b). Moreover, PCM should be non-toxic and non-flammable to avoid unsecured operation conditions. Finally, it is needed to be cheap, abundant, and financially sustainable.

3.1. Classification Of PCM

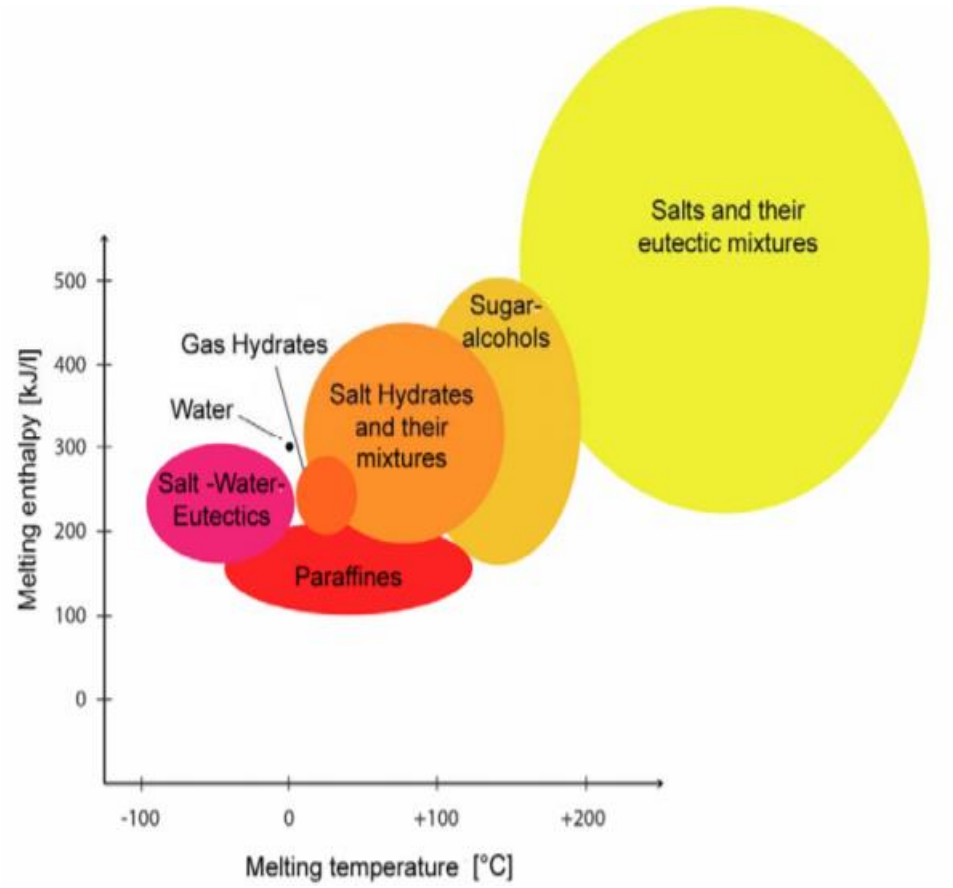

Figure 3.1. Types of PCM grouped in different melting temperature and enthalpy scales (Source:(“(No Title)” n.d.))

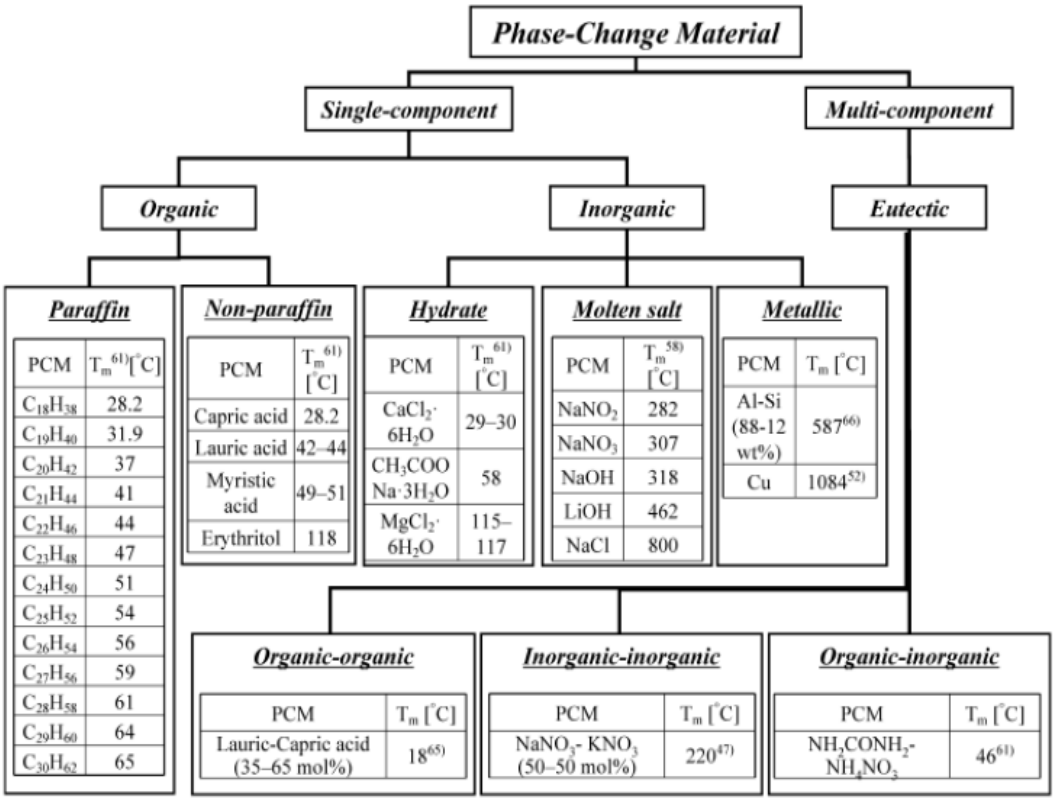

Figure 3.2. Categorization of PCM with the comparison of melting temperatures (Source:(Kenisarin 2010))

Phase change materials can be categorized under three groups: organics, inorganics, and eutectics. Unfortunately, the materials are insufficient to answer all the property requirements above. The advantages and disadvantages of each material should take into consideration during PCM selection. It is possible to find PCMs that have different fusion enthalpies and melting temperatures in wide range, as can be seen from Fig. 3.1. Figure 3.2 introduces PCM types, its subgroups and gives specimens.

Organic PCMs consists of paraffins and non-paraffins. Paraffins (C_nH_{2n+2}) are basic hydrocarbon compounds and are produced by distillation of petroleum. With an increase in the number of carbon and hydrogen atoms for any selected paraffin, it melts at higher temperatures. The other organic PCM group non-paraffins consist of sugar alcohols, fatty acids, and esters. They are obtained from food-based products. Specifically, sugar alcohols and Erythritol will be handled in Section 3.2. Organic PCMs show good thermal stability, low corrosive, and toxic effects, but they suffer from low fusion enthalpy and poor thermal conductivity.

Another group inorganic PCMs contain three subgroups: metallic, salt hydrate, and molten salt. Low melting metals like gallium (T_m=29.76°C) or medium melting metals like tin (T_m=231.9°C) were studied before for the purpose of understanding melting/solidification processes(Gau and Viskanta 1986; Wolff and Viskanta 1987). As for high-temperature range, metals are known as heat transfer fluids in nuclear power plants. The thermal conductivity of metals and their alloys are substantially high. For example, Zinc-Tin alloy (70%-30%) has a thermal conductivity of approximately 50 W/mK in liquid form(Adinberg, Zvegilsky, and Epstein 2009). Hence, they can be seen conceivable as PCM, yet are stayed out of TES applications because of their large weight. Salt hydrates ($AB.xH_2O$) are prominent inorganic PCMs due to lack of poor conductivity and their relatively high fusion enthalpy in comparison to most of organic PCMs. However, salt hydrates demonstrate weak thermal stability and corrosive effects on the surface of heat exchangers, fins, and containers. As from molten salts, nitrite and nitrates of sodium and potassium are preferred materials, especially for CSP-TES applications in the medium temperature range (120-320°C). Organic PCMs fall back with their low conductivities compared to inorganics, but inorganics have disadvantages of high supercooling and phase segregation in general.

Finally, eutectics are binary or ternary combinations of organic and/or inorganic PCMs. There are some examples of eutectic in the Fig. 3.2. Eutectics are prepared to activate properties of each constituent and have unprecedented melting points.

3.2. Erythritol As A Promising PCM

Sugar alcohols from organic PCMs are family members of carbohydrates group which have low molecular weight. Out of the TES function, general utilization fields are the food and pharmaceutical sector. They are produced commonly by reduction reactions of carbohydrates while some fruits and vegetables involve them naturally. Sugar alcohols have outstanding features. Latent heat capacity of sugar alcohols is 2-3 times higher than paraffins that work at the same temperature range, as seen in Fig. 3.1. Also, they are not flammable, corrosive and toxic. The most commonly studied ones are xylitol, adonitol, l-arabitol, d-mannitol, and erythritol, whose latent heat capacities and melting temperature ranges are 250 to 340 kJ/kg and 95 to 167°C, respectively(del Barrio et al. 2017). Although salt hydrates are superior to organic PCMs due to higher fusion enthalpy of

inorganic PCMs in general, sugar alcohols are competitive owing to these thermophysical properties.

Among sugar alcohols, Erythritol ($C_4H_{14}O_4$) is a very promising PCM with the highest fusion enthalpy $L_{erythritol}$=339 kJ/kg. It took place in absorption cooling(Agyenim 2016), waste heat of diesel engine(Zeng et al. 2017), solar box cooker(Coccia et al. 2020) applications in literature. Also, its performance was investigated in spherical capsules, vertical and horizontal arranged heat exchangers before (Junior et al. 2018; Nazzi Ehms et al. 2018; Agyenim, Eames, and Smyth 2010; Y. Wang et al. 2016). Erythritol, which has a melting temperature of 117 ° C, attracts the attention of solar-powered ORC and domestic hot water applications.

Table 3.1. Comparison of selected medium temperature range phase change materials (Source:(Agyenim, Eames, and Smyth 2010))

Property	Phase Change Material (PCM)		
	Erythritol	$MgCl_2.6H_2O$	RT100
Melting Temperature, T_m [°C]	117.7	116.7	99
Latent Enthalpy, L [kJ/kg]	339.8	168.6	168
Specific Heat (Liquid), c_p [kJ/(kg.K)]	2.8	2.6	2.4
Specific Heat (Solid), c_p [kJ/(kg.K)]	1.4	2.3	1.8
Thermal Conductivity (Liquid), k, [W/(m.K)]	0.3	0.6	0.2
Thermal Conductivity (Solid), k, [W/(m.K)]	0.7	0.7	0.2
Density (Liquid), ρ, [kg/m^3]	1300	1450	770
Density (Solid), ρ, [kg/m^3]	1480	1570	940

Table 3.1 shows the comparative thermophysical properties of selected PCMs available for medium temperature range applications. Erythritol, $MgCl_2.6H_2O$, RT100 are group members of sugar alcohols, salt hydrates, and paraffin, respectively. As an organic PCM, the thermal conductivity of Erythritol is higher than RT100. When looked at the table, Erythritol and $MgCl_2.6H_2O$ melt almost at the same temperature. Erythritol falls behind at the performance of conductance relative to $MgCl_2.6H_2O$, but its latent heat capacity is approximately two times greater than $MgCl_2.6H_2O$. These thermophysical properties make Erythritol a privileged PCM for medium temperature range.

The disadvantage of Erythritol is supercooling. The supercooling phenomena can be considered as an advantage or disadvantage depending on the application whatever is

short- or long-term. This phenomenon makes the advantage of avoiding heat loss for long-term applications in which periods might be defined in weeks or months. On the other side, supercooling is an undesired PCM feature for short-term applications.

3.3. Thermal Conductivity Enhancement (TCE) Methods

There are several ways to utilize PCM in energy systems. Recently being popular technology is encapsulation. The idea is that PCMs are encapsulated inside spherical or cylindrical capsules in large numbers so that faster charging and discharging become possible since the high ratio of heat transfer area to PCM volume is obtained. Encapsulation techniques provide capsules at macro-, micro- or nano-scale. Regarding volume expansion of PCM, stiff or flexible macro-capsules can be contemplated. In stiff capsules, an air gap should be allocated to let PCM expand. There is no need such a space for flexible capsules, but this option is not feasible and cost-effective for high-temperature storage. While plastic capsule shells are suitable to work in low-temperature applications, shell materials are chosen from metal for the high temperatures. The disadvantages of encapsulated PCMs, especially at the micro- and nano-scale, are being expensive and not easy-manufacturable. Also, using metal shells limits the applicability due to its high weight(Steinmann and Tamme 2008).

Multiple PCM utilization in a cascaded heat exchanger is another approach which promotes the system efficiency. The employment of multiple PCMs results in a nearly constant temperature difference and so constant heat flux throughout the heat transfer area. Along flow direction inside HTF tubes, the temperature of the fluid and temperature difference between the HTF and PCM decreases gradually. While a high melting rate and overheating at the entrance region of single-PCM heat exchangers, melting efficiency is relatively low for the remainder of the heat exchanger. However, in each division of cascaded heat exchangers, melting temperatures of filled PCMs are in descending sequence along the flow direction. Thus, higher heat transfer rates and exergy efficiency are achieved(Kalapala and Devanuri 2018).

The most severe thing that TES systems suffer is poor conductance of PCMs. Substantial attempts have been devoted to studying thermal conductivity enhancement (TCE) methods. Although PCM systems enable relatively high thermal energy storage capability, they come with the burden of relatively low thermal conductivity. Therefore,

the literature documents the research on thermal conductivity enhancement (TCE) on PCM in two major class: active and passive. Active TCE techniques require additional energy input such as electrical, rotational(Kurnia and Sasmito 2018), ultrasonic(Zhang and Du 2018), etc. Passive TCE techniques can be categorized under three groups, which are increasing of overall PCM conductance, extended surfaces, and variation in tube shapes and orientations.

The first technique to increase the overall conductance, embedding porous matrix medium inside PCM, is investigated by Liu et al.(Z. Liu, Yao, and Wu 2013). Although the foam prevents natural convection to a large extent, it helps the melted PCM region to distribute heat by fast conduction. Low porosity and high PPI (pore per inch) foam conditions are beneficial for the melting process. However, metal foams may experience heavy corrosion when used inside salt hydrates. In the study of Zhao and Wu(Zhao and Wu 2011) in which porous foam and expanded graphite compared, the foam was preferable because it does not suppress natural convection as much as expanded graphite does, but it is estimated that using foams causes an increment in the cost about 10-20%.

Adding high thermal conductive nano-particles is the second way to increase the overall PCM conductance. The thermal conductivity enhancement ability of the nanoparticles varies depending on adding ratio, congruence between PCM and nanoparticle, and physical properties (e.g., particle size, shape). The most common nano-additives are metal oxides and carbon-based materials. Since metal oxides pose weight problems, carbon-based materials with their properties of being thermal and chemical stabilities became attractive. Expanded graphite, graphene nanoplatelets (GNP), carbon nanotube (CNT) are examples of carbon-based nanoparticles. Apart from the enhancement of thermal conductivity, nano-particles are quite effective in eliminating the supercooling. Owing to uniform heat diffusion throughout the melted PCM, the supercooling degree drops remarkably. However, carbon-based nanoparticles tend agglomeration and sedimentation, decrease latent heat capacity per unit volume, and increase the viscosity of PCMs(Qiu et al. 2019).

The extended surfaces is the most applied TCE method in literature. The implementation of fins made of high conductive materials is one of the most promising methos in comparison to the others, with the advantages of low cost, accessibility, and ease in manufacturability. Hence, the employment of fin structures in the LHTES units has gained the attraction of many researchers(Deng, Nie, Wei, et al. 2019)(Deng, Nie, Wei, et al. 2019; Rozenfeld et al. 2015; P. Wang et al. 2016; Kazemi et al. 2018; C. Liu

and Groulx 2014; Deng, Nie, Jiang, et al. 2019; Mat et al. 2013; Joybari et al. 2017; Tao and He 2015; Rathod and Banerjee 2015; Ji et al. 2018; Sciacovelli, Gagliardi, and Verda 2015; Vogel and Johnson 2019; Pizzolato et al. 2017; Hosseini et al. 2015; Cao, Yuan, Xiang, Sun, et al. 2018). In brief, longitudinal fins show better melting performance than circular radial fins in both horizontal and vertical oriented heat exchangers. Increase in fin length and number of fins accelerates the melting due to larger heat transfer area, but fin thickness does not have significant enhancement in the melting performance. For each boundary condition, different optimal fin numbers exist. Moreover, using fins becomes more effective at lower temperature difference between the PCM melting temperature and boundary temperature. However, fins inhibit the convection circulations of PCM dramatically, especially in horizontal oriented heat exchangers.

The other approach to obtain extended surfaces is to use multitube heat exchangers whose triggering melting effect was proven experimentally and numerically by many studies (Kousha et al. 2019; Jourabian, Farhadi, and Rabienataj Darzi 2017; M. Esapour et al. 2016). Moreover, when the total heat transfer area is kept constant, the utilization of multiple tubes shows greater performance compared to fin insertion. Parry et al.(Parry, Eames, and Agyenim 2014) numerically documented the effect of fin type and tube number for PCM applications. The results show that, even though the HTF-PCM contact surface area of the multi-tube case is 55% smaller than the longitudinal finned-tube case, the PCM melts 37% faster compared to the others. Besides, in the natural convection dominated process of melting, the irreversibility is dependent on the number of HTF tubes. With an increase in the number, heat is transferred more efficiently, unlike single-tube heat exchangers in which heat is distributed only from one source. Then, less irreversibility is obtained in the melting process(De Lucia and Bejan 1991).

There are dual approaches in literature such as multitube-fin, multitube-porous foam, fin-nanoparticle, etc (Dandotiya and Banker 2017; Shinde et al. 2017; Bhagat, Prabhakar, and Saha 2018; Niyas, Prasad, and Muthukumar 2017; Raul, Bhavsar, and Saha 2018). No constraint exists to apply multiple methods for conductivity enhancement. But, the addition of each method occupies space in the melting domain and causes a reduction in heat storage capacity for the given volume. The study of Parsazadeh and Duan(Parsazadeh and Duan 2018), in which both nanoparticle and fin enhancement methods are applied, showed that since each method aggravates the natural convection-driven heat transfer, it is better to cancel nanoparticle addition. In the study of Esapour et al.(Mehdi Esapour et al. 2018), multitube/porous foam methods are investigated together.

They found that while the increase in the number of the tubes affects mostly the melting rate, metal foam is more effective rather on the solidification process. Also, the authors reported that tube arrangement does not state an impact on melting or solidification due to the suppression of natural convection.

Overall, when these methods mentioned above are reconsidered, it is seen that not only conduction heat transfer is enhanced significantly but also natural convection of melted PCM is suppressed. The ways to enhance the melting process by natural convection is by varying the shape of the shell tube and the location of the HTF tube. From the view of practical sense, increasing eccentricity by moving the tube vertically down to where pure conduction occurs is quite a remarkable approach because it makes more space for natural convection to be more effective in proportion to Rayleigh number(Jourabian et al. 2013; Dhaidan et al. 2013; Yusuf Yazici et al. 2014; Dutta, Atta, and Dutta 2008; Pahamli et al. 2016; Cao, Yuan, Xiang, and Highlight 2018; Darzi, Farhadi, and Sedighi 2012; Zheng, Xu, and Li 2018). There are limited studies on the effect of the shape of the shell and HTF tube. For instance, Faghani et al.(Faghani, Hosseini, and Bahrampoury 2018) employed elliptical cylinders for the HTF tube with the variable orientation of the cylinders. Their simulations showed that horizontal and vertical orientations for inner and outer tubes, respectively, yields a decrease in melting time. Besides, the liquid front showed that the configuration leads the melting front to develop in the side regions of the domain. Vogel et al.(Vogel, Felbinger, and Johnson 2016) documented that the effect of natural convection becomes dominant on heat transfer as width of the enclosure increases and the height decreases for eutectic mixture of potassium nitrate and sodium nitrate (KNO_3-$NaNO_3$). Seddegh et al.(Seddegh, Wang, and Henderson 2016) also documented the effect of orientation of the shell and tube heat exchangers on the melting time of PCM. Their results showed that natural convection dominates the upper region of the tube whereas conduction dominates the bottom region. They also documented the effect of HTF inlet temperature plays an integral role in thermal energy storage where the effect of mass flow rate is not that essential. Luo et al.(Luo et al. 2015) documented the effect of HTF tube location on melting behavior of PCM by using lattice-Boltzmann method. The tubes were arranged in centrosymmetric, inline and staggered with fixed numbers of HTF tubes and PCM volume. The results revealed that since tubes do not inhibit flow of melted PCM and they are well-distributed in the PCM domain, the melting rate of centrosymmetric alignment is better than the other competing cases.

The majority of the studies carried out were focused on phase change processes of low-temperature applications. As for PCMs whose melting temperature is above 100°C, there exist rare publishes. Literature shows that the melting time of a TES system using erythritol as PCM can be decreased by altering the shape of the shell and positions of HTF tubes. However, literature does not discuss the physical reasons why the competing designs were selected. Here, the aim is to rely on design improvements on the shape of shell tube and positions of HTF tubes by considering the physics of the process, i.e., melted region characteristics based on conductive and convective heat transfer. Literature also lacks in documenting how the S-curve of melting varies based on design alterations in multitube configurations. It is also discussed how the S-curve of melting becomes steeper with design alterations based on the proposed methodology.

CHAPTER 4

NUMERICAL MODEL

4.1. Numerical Model

Heat exchangers are essential components for many different engineering systems like the power plant, heating and cooling cycles, chemical separators, etc. Thus, the design of heat exchangers is the primary issue in order to establish feasible systems. To apply experimental procedures for the investigation of design and optimization problems might be high-costly and time-consuming because many geometric design parameters should be concerned. That's why computational fluid dynamics (CFD) is a favorable method.

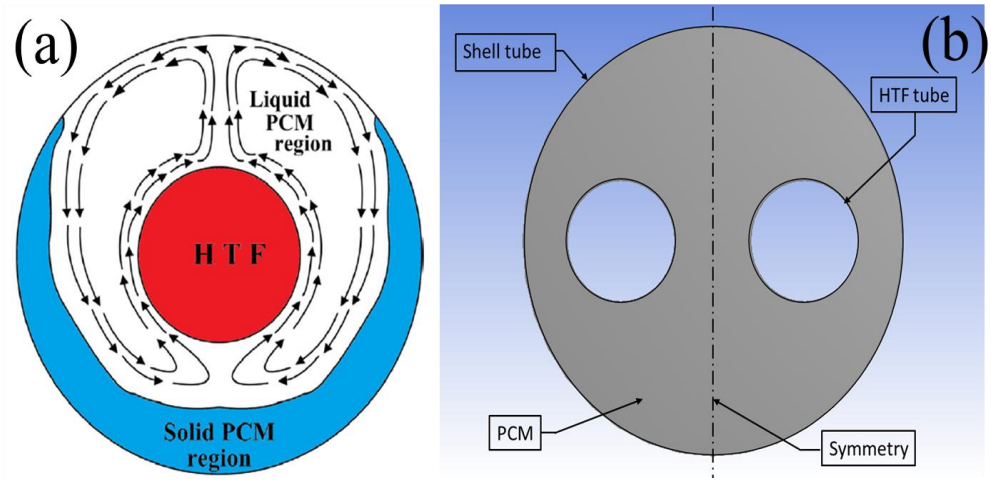

Figure 4.1. (a) flow regime of liquid PCM inside a horizontal arranged shell-and-tube heat exchanger (Source:(Y. Wang et al. 2016)), and (b) geometry of the base design

Figure 4.1a illustrates how the melted liquid in PCM domain circulates for a horizontally arranged shell-and-tube heat exchanger. Figure 4.1b shows the base design

which has two inner HTF tubes with outer shell tube. The diameters of the inner and outer tubes are 28.28 mm and 100 mm, respectively. The distance of each inner tube to the symmetry line is 10 mm. PCM (i.e., erythritol) is located inside the annulus region bounded by shell tube and the thermophysical properties of erythritol are listed in Table 4.1. Erythritol is selected because its capability for latent energy storage, and it has no toxic and corrosive effects.

Table 4.1. Thermophysical properties of Erythritol as PCM
(Source:(Parry, Eames, and Agyenim 2014))

Parameter	Value
ρ_{ref} [kg/m^3]	1480
μ [kg/(m.s)]	0.01 constant
k [W/(m.K)]	0.733 at 20 °C, 0.326 at 140°C (linear distribution)
C_p [kJ/(kg.K]	1.38 solid and 2.76 liquid (linear distribution)
L [kJ/kg]	339.8
$T_{solidius}$ [°C]	116.7
$T_{liquidius}$ [°C]	118.7
β [1/K]	0.001014

Here, it is assumed that the liquid phase of PCM is a Newtonian fluid, phase change occurs in isothermal condition ($T_{solidius}$ =$T_{liquidius}$ =117.7°C), and the effect of viscous dissipation is neglected. Maximum Rayleigh number is 7.92×10^6, so flow is laminar during the melting process.

The outer shell wall is assumed as adiabatic because of negligible heat loss in LHTES units due to their well-insulated nature. Inner HTF tube walls are assumed to be constant at 136.7°C. The PCM is initially subcooled 1°C below its melting temperature; therefore, the difference between the initial temperature of PCM and HTF tubes is 20°C.

The numerical studies were conducted by using a commercial computational fluid dynamics software, i.e. ANSYS 19.0("ANSYS Fluent Software | CFD Simulation" 2019). SIMPLE algorithm was used for pressure-velocity coupling. The convergence criteria are 10^{-5} for conservation of mass and momentum equations and it is 10^{-10} for conservation of energy equation. Time step during simulations is 0.05s to uncover the effect of convection accurately. We also confirmed that the time step is small enough which does not affect the results. For instance, as the time step increased from 0.05s to 1s maximum deviation becomes 1.49%.

4.2. Governing Equations

ANSYS Fluent is software that approaches the finite volume method. The software involves solidification/melting module, and transient solid-liquid phase change problems are simulated with enthalpy-porosity technique(Brent, Voller, and Reid 1988). Based on the simplifications, conservation equations of mass, momentum along x- and y-direction can be described in 2D space as below:

$$\frac{\partial \rho}{\partial t} + \nabla(\rho \mathbf{u}) = 0 \tag{4.1}$$

$$\frac{\partial(\rho u)}{\partial t} + \nabla \cdot (\rho \boldsymbol{u} u) = \nabla \cdot (\mu \nabla \mathrm{u}) - \frac{\partial P}{\partial x} + Au \tag{4.2}$$

$$\frac{\partial(\rho v)}{\partial t} + \nabla \cdot (\rho \boldsymbol{u} v) = \nabla \cdot (\mu \nabla \mathrm{v}) - \frac{\partial P}{\partial y} + Av + S_b \tag{4.3}$$

where **u,** is the velocity vector, whose components are u and v along x- and y-directions, respectively. ρ, μ, P, and T is density, dynamic viscosity, pressure, and temperature, respectively. Also, the buoyancy source term is as below:

$$S_b = \rho_{ref} g \beta (T - T_{ref}) \tag{4.4}$$

Here, ρ_{ref}, g, β, and T_{ref} are reference density, acceleration of gravity, coefficient of volumetric thermal expansion, and reference temperature, respectively. The region particular to the melting/solidification model, is called the mushy zone, is defined by Brent et al.(Brent, Voller, and Reid 1988) as the dispersion of melted liquid inside dendritic solid PCM. That region is in neither solid nor liquid form. Fluent identifies the mushy zone region as a pseudo-porous medium. While the porosity goes from 0 to 1, PCM melts, or it solidifies from 1 to 0. The material is recognized as in mushy form when the porosity is between 0 and 1. Au and Av, momentum dissipation source terms, have a function that serves for suppressing velocity of PCM when it is in solid or mushy form and are added to the conservation of momentum equations to mimic Carman-Kozeny relation as if the PCM domain is a porous medium. A term is called porosity function, defined as:

$$A = -C \frac{(1-f)^2}{f^3 + b} \tag{4.5}$$

Here, parameter f is the liquid fraction that supersedes of porosity term in Carman-Kozeny relation. C, is mushy zone constant, equals 10^5 kg/(m^3.s). Mushy zone constant exists for how fast phase change will occur, and forms the shape of the melting front. It changes between 10^3 and 10^8 kg/(m^3.s)(Brent, Voller, and Reid 1988). Mushy zone constant in high values leads to slower fluid velocities and a decrease in phase change rate. It is more pronounced in natural convection dominant processes, so mushy zone constant should be defined in the perspective of how much natural convection dominates the process. b equals 0.001 and is inserted to the denominator to avoid division by zero in the case of fully solid PCM.

The energy equation is

$$\frac{\partial(\rho h)}{\partial t} + \nabla \cdot (\rho \boldsymbol{u} h) = \nabla \cdot (k \ \nabla T) + S_h \tag{4.6}$$

and energy source term, S_h, is added to establish effects that come with phase change.

$$S_h = \frac{\partial(\rho \ \mathrm{h_l})}{\partial t} + \nabla(\rho \boldsymbol{u} \ \mathrm{h_l}) \tag{4.7}$$

The melt interface is tracked implicitly by governing enthalpy term in the energy equation instead of the temperature. Here, k is thermal conductivity. Enthalpy, h, comprises of two energy contents: sensible (h_s) and latent (h_l). The summation of the contents is represented as:

$$\begin{gathered} h = h_s + \mathrm{h_l} \\ \text{where } h_s = \int_{T_{ref}}^{T} c_p \ \mathrm{dT} \quad \text{and } h_l = fL \end{gathered} \tag{4.8}$$

$$h = \begin{cases} \displaystyle\int_{T_{ref}}^{T_{solidius}} c_p \ \mathrm{dT} & \text{if } \mathrm{T} < \mathrm{T}_{solidius} \\ \displaystyle\int_{T_{solidius}}^{T_{liquidius}} c_p \ \mathrm{dT} + \mathrm{f\ L} & \text{if } \mathrm{T}_{solidius} < \mathrm{T} < \mathrm{T}_{liquidius} \\ \displaystyle\int_{T_{liquidius}}^{T} c_p \ \mathrm{dT} & \text{if } \mathrm{T}_{liquidius} < T \end{cases} \tag{4.9}$$

PCM temperature ranges are seen in equation (4.9): the temperature value, respectively, is lower than solidus temperature, is between the solidus and liquidus, and is higher than the liquidus. Here, the conditions, respectively, represent sensible heating

of solid PCM, phase change and sensible heating of PCM in mushy form, and sensible heating of melted PCM.

4.3. Validation, Mesh And Time Independency

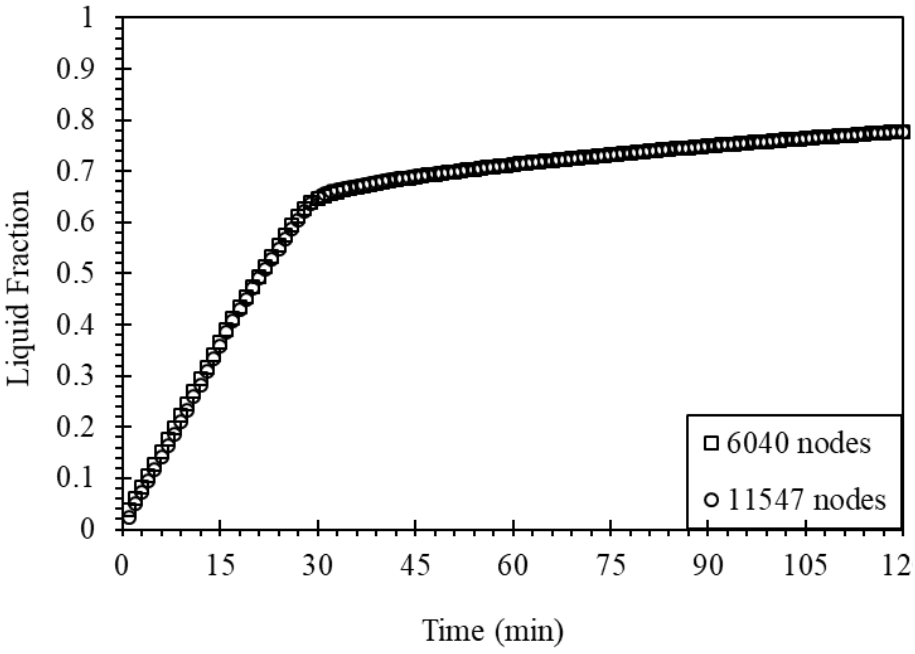

Figure 4.2. Grid independency test

Figure 4.2 documents the effect of grid size is negligibly small for the entire time span with the domains consist of 11547 and 6040 nodes, respectively. Please also note that quadrilateral mesh is used. The computer that simulations were carried out consists of 40 GB of RAM and two 12-core Intel® Xenon®E5-2630 CPUs. Each simulation in Fig. 4.2 requires around 4.7 million iterations which took almost five days (~120hours) with the specified computer. Therefore, the simulations were ceased when fraction of melted substance is greater than 75%. Figure 4.2 also shows that speed of phase change decreases greatly around 30th minute where conduction becomes dominant heat transfer mechanism.

Figure 4.3 shows that the results of current study and Parry et al.(Parry, Eames, and Agyenim 2014) are in agreement. The figure also shows that melting time, when the slope of curve, changes is accurately documented in the current numerical method.

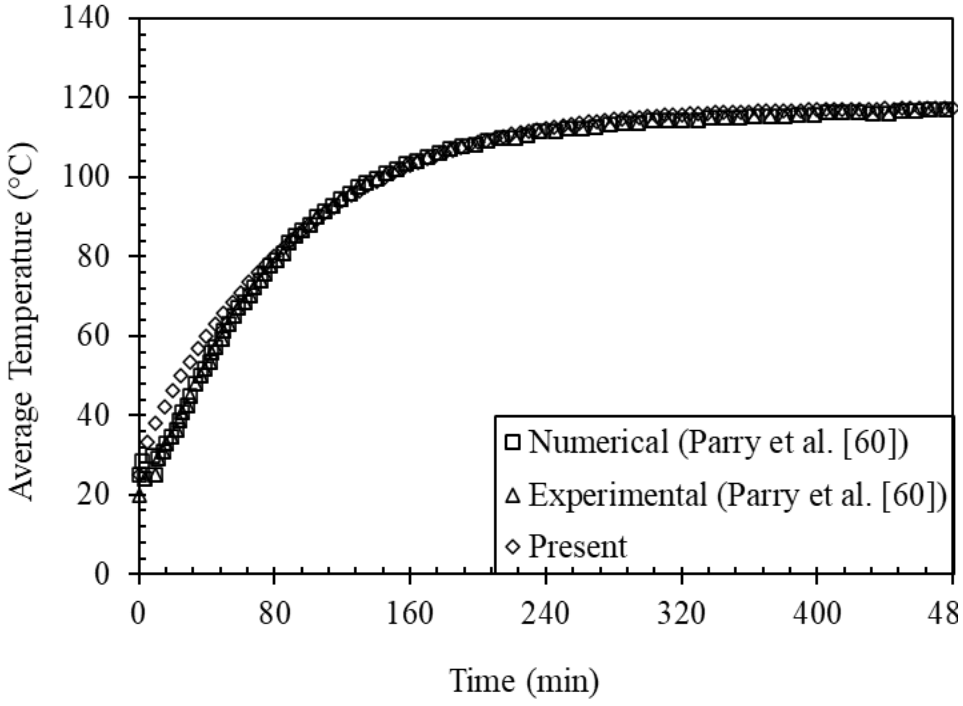

Figure 4.3. Comparison of the current study results with the results of Parry et al.(Parry, Eames, and Agyenim 2014)

CHAPTER 5

NUMERICAL RESULTS

5.1. Two HTF Tubes In A Circular Shell

Consider two HTF tubes inserted in a circular shell as shown in Fig. 4.1b. Figure 5.1 shows the development of liquid fraction contours for five distinct time. The contours represent how the liquid melts almost from 0 volume fraction to the time when melting speed decreases greatly. First, the main heat transfer mechanism is conduction and melted region thickness grows gradually in both x- and y-directions, i.e. as can be seen in Fig. 4.1 2nd minute. Then natural convection dominates melting due to increased buoyancy force which is driven by the density field and gravitational acceleration. The melted region becomes asymmetric as the convection mechanism begins, i.e. thicker melted region above the HTF tube as can be seen in Fig. 5.1 10th minute. The melted regions around HTF tubes do not affect each other until the time when they intersect at 16th minute. Then, melted speed decreases as can be seen in Fig. 5.1. This implies transferred energy is stored as sensible enthalpy rather than latent one. Last but not least, as the region above HTF tubes melt entirely, melting process is dominated by the conduction which occurs below the HTF tubes. In order to uncover these transitions, variations of liquid fraction, latent/sensible enthalpy ratio and sensible enthalpy based on time is shown in Fig. 5.2.

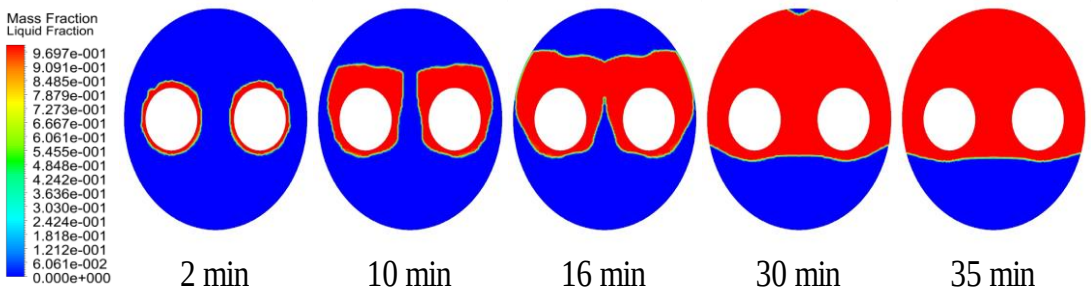

Figure 5.1. Evolution of liquid fraction contours for two-tube base case

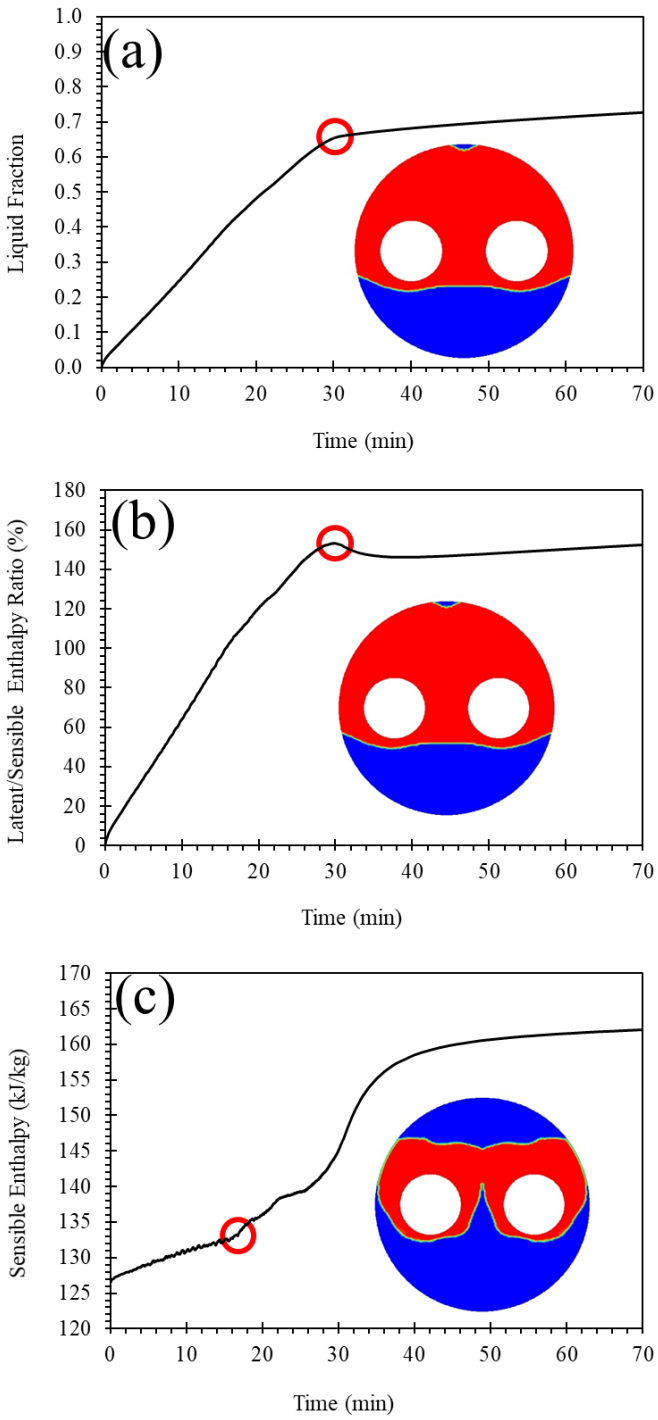

Figure 5.2. Transient variation of (a) liquid fraction, (b) latent/sensible enthalpy ratio and (c) sensible enthalpy of LHTES system for two tube-base case

Figure 5.2 also shows the contour of liquid and solid substance distribution where they are represented with red and blue colors, respectively. Figure 5.2a shows 65% of the substance melts in 30 minutes, and melting from 65% to 73% takes 40 more minutes. The

characteristics of liquid fraction is an S-curve. Figure 5.2b shows that the ratio of the latent enthalpy decreases as the heat transfer mechanism becomes pure conduction again at 30th minute. After that time, melting rate decreases dramatically and the ratio of sensible enthalpy enhances greatly as can be seen in Fig. 5.2c. Figure 5.2c also shows that the amount of sensible heat begins to increase greatly when two melted regions around HTF tubes intersect. Therefore, removing the regions where solid melts slowly may increase the process speed. The S-curve of melting is aimed to become steeper as discussed in Ref. (Cetkin, Lorente, and Bejan 2012).

5.2. Two HTF Tubes In A Rectangular Shell

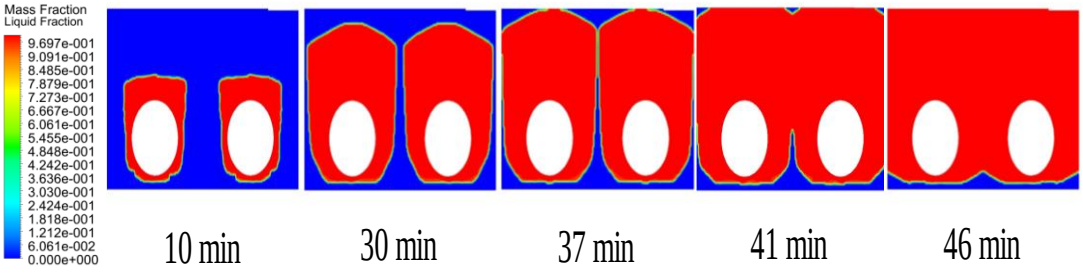

Figure 5.3. Evolution of liquid fraction contours for two-tube with rectangular shell

The results of Fig. 5.2 document that the melting process slows down and the majority of the stored energy becomes the sensible one after the melted regions intersect. Therefore, it can be concluded that alteration in shell shape may yield melting process to continue with the speed before intersection time. The results also show that before the intersection time melting in tubes does not affect each other due to their symmetrical nature. The shell design can be improved with the displacement of liquid regions around HTF tubes, i.e. packing melted regions into a domain. Figure 5.2c shows that the melted regions become almost a rectangular region where the tubes are located near the bottom of the rectangle. Please note that the volume of the PCM material and HTF tubes are kept constant. Therefore, the distance between each inner tube, the symmetry line and the outer tube raises from 10mm to 15mm. The distance from the bottom of the shell to the inner tubes is 5mm.

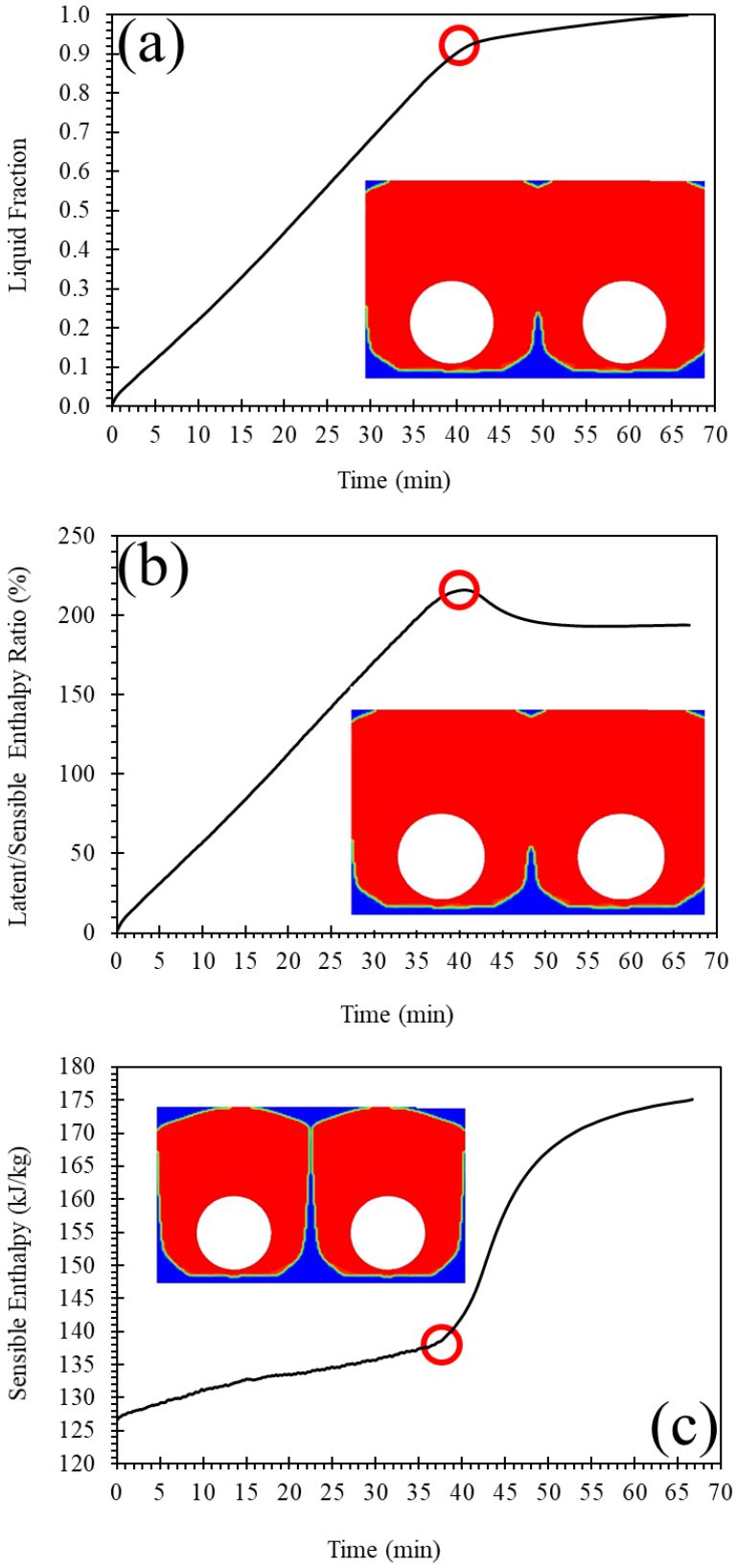

Figure 5.4. Transient variation of (a) liquid fraction, (b) latent/sensible enthalpy ratio and (c) sensible enthalpy of LHTES system for two-tube with rectangular shell

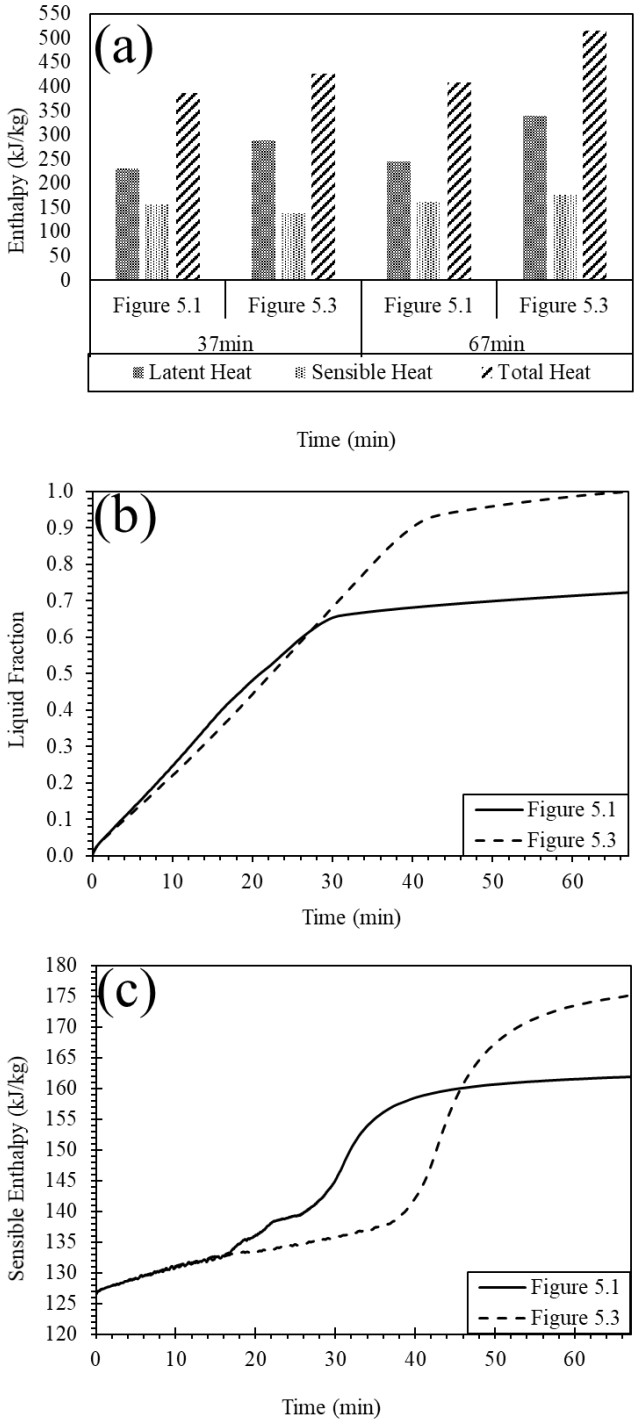

Figure 5.5. Comparison of two-tube cases in Fig. 5.1 and Fig. 5.3 for (a) total enthalpy, (b) liquid fraction and (c) sensible enthalpy

Then, sensible enthalpy starts to rise in a steeper trend as happened in the base case as shown in Fig. 5.2c. Figure 5.4b also documents that the latent enthalpy ratio decreases as the region above tubes is melted similarly. However, Figure 5.4a also shows

more than 90% of PCM is melted unlike the 65% of previous case. Figure 5.4c also shows increase in sensible heat is postponed greatly with shell design alteration. This accelerates the melting rate greatly, but there is still solid PCM. Rectangular design satisfies 92% of PCM to melt quickly by natural convection in the first 41 minutes, but melting of the rest requires additional 25minutes.

Figure 5.5 uncovers the advancement of rectangular shell design relative to the base design. Figure 5.5a shows the amount of sensible and latent enthalpies for the base design of Figure 5.1 and the improved design of Fig. 5.3. It shows that the amount of latent enthalpy increases 20% and 27.7% for 37^{th} and 67^{th} minutes, respectively, but while the amount of sensible enthalpy is 11.9% lower at 37^{th} minute, it is 7.5% higher at 67^{th} minute. In addition, due to the decrease in thermal resistance, total stored enthalpy also increases 9.2% and 20.8% for 37^{th} and 67^{th} minute. This also explains why sensible enthalpy storage of Fig. 5.3 becomes greater at the 67^{th} minute. Figure 5.5b shows that the S-curve of melting becomes steeper with the improvements on the shell design. Figure 5.5c shows the sensible enthalpy storage in designs of Figs. 5.1 and 5.3 are the until 16^{th} minute. Then, sensible heat storage increases rapidly in the design of Fig. 5.1 because the melted regions intersect and the rate of increase diminish. Whereas the melted regions intersect at the 37^{th} minute for the design of Fig. 5.3, and sensible heat storage increases rapidly and becomes greater than the one for the design in Fig. 5.1. However, Figure 5.5a shows this increase in sensible heat relatively small in comparison to the total heat storage and increment in the latent heat storage.

5.3. Four Concentric Tubes In A Circular Shell

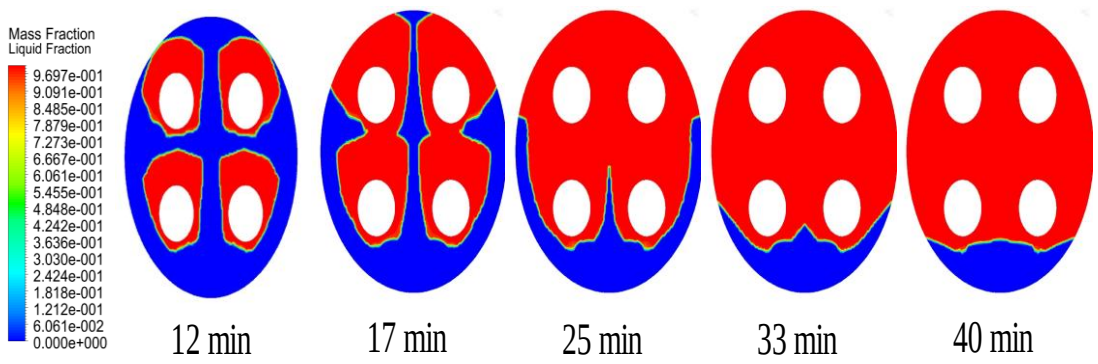

Figure 5.6. Evolution of liquid fraction contours for four-tube concentric case

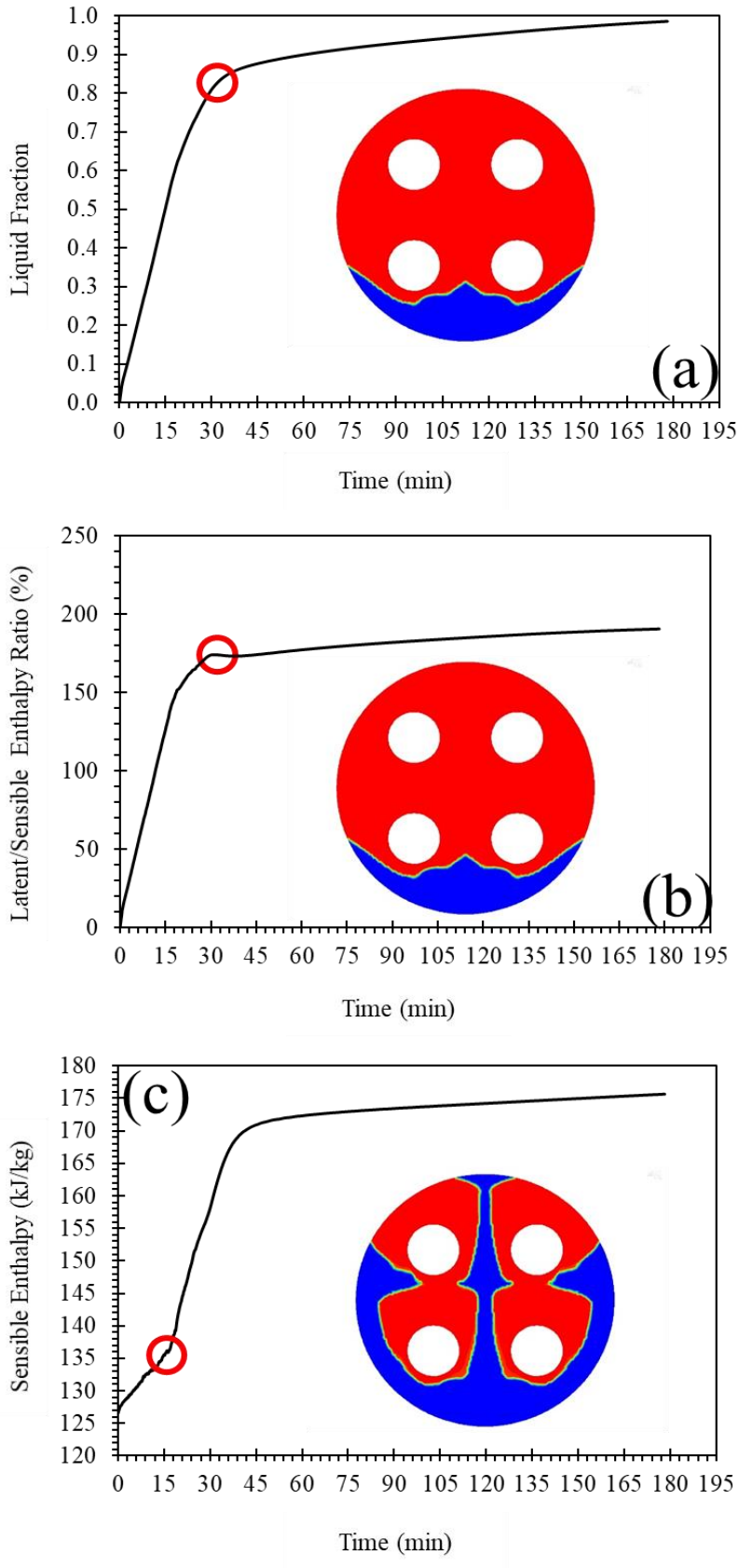

Figure 5.7. Transient variation of (a) liquid fraction, (b) latent/sensible enthalpy ratio and (c) sensible enthalpy of LHTES system for four-tube concentric case

Consider four HTF tubes inserted in a circular shell in concentric manner as shown in Fig. 5.6. The volume of PCM and tubes are the same with previous sections. However, because there are four tubes the heat transfer surface area increases.

Increase in melting rate is expected in four tube case due to increase in the heat transfer surface area. However, the design is concentric, therefore, the bottom of the shell is further from surface of the tubes. This yields conduction to be dominant in the melting of bottom region as in the design of Fig. 5.1. Figure 5.6 shows that at 12th minute of the melting process, growth of the melted region is limited by the outer tube and at 17th minute, the melted liquid of the upper and lower tubes touch with each other. After 33rd minute, the melting by natural convection diminished, and the process passes to the plateau stage as shown in Figs. 5.7a and 5.7b. In the first 33 minutes, 83% of the PCM melts where the rest requires additional 145 minutes. In addition, Figure 5.7c shows sensible enthalpy begins to increase rapidly after 17th minute (i.e. when the melting regions intersect) and increases even more after 33rd minute.

5.4. Four Eccentric Tubes In A Circular Shell

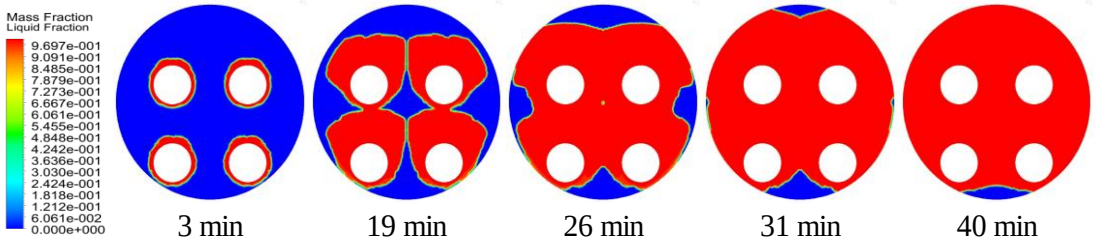

Figure 5.8. Evolution of liquid fraction contours for four-tube eccentric case

Consider HTF tubes in Fig. 5.6 moved down to enhance melting rate as shown in Fig. 5.8, i.e. tubes were shifted 11 mm downward without changing the arrangement.

Figure 5.8 shows that melted regions of the tubes located below touches to the shell at the 3rd minute of process. The liquid layer of each tube grows individually until they combine at 19th minute. On the contrary to previous cases, sensible enthalpy begins to increase rapidly when melted liquid layers of all tubes melt PCM located in the center of the shell at 26th minute. Here, the time of the melting process to pass to the plateau stage is 31th minute as can be seen in Figs. 5.9a and 5.9b. Figure 5.9c also confirms the

rapid sensible energy storage begin at the 26th minute. The liquid fraction contours of Fig. 5.8 show that removing some regions from the shell may increase the melting rate as in two tube cases.

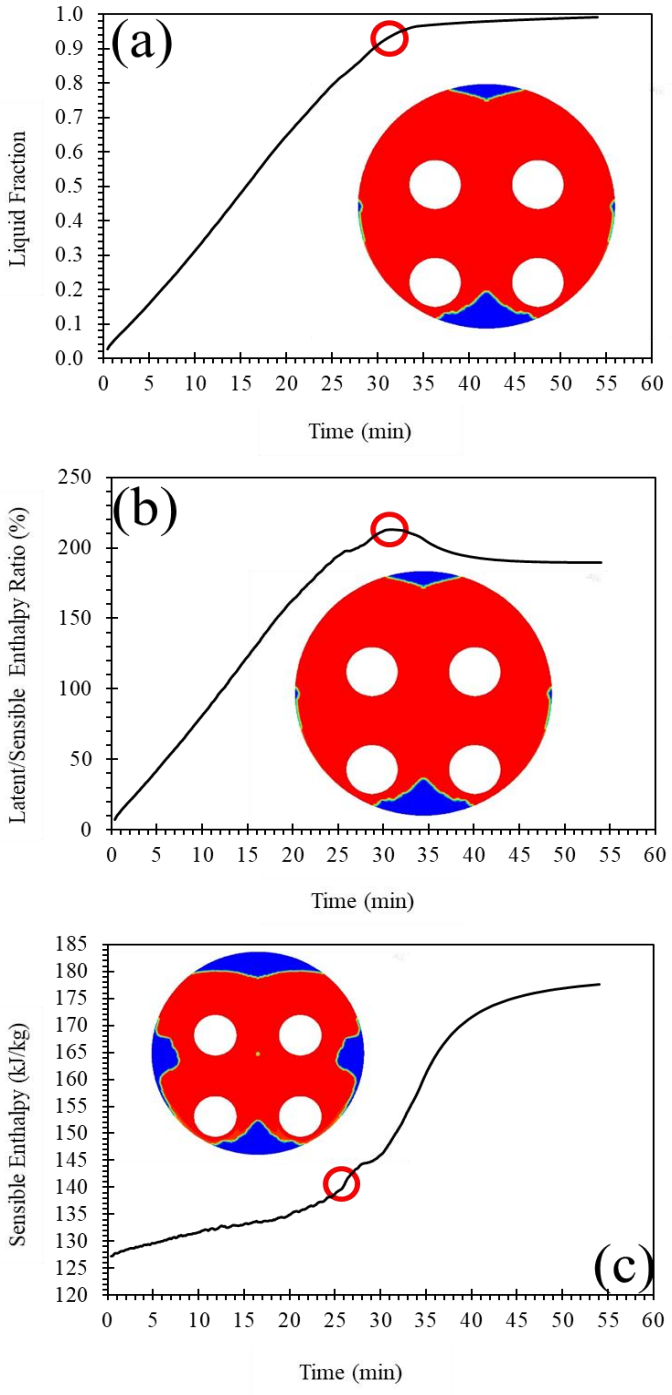

Figure 5.9. Transient variation of (a) liquid fraction, (b) latent/sensible enthalpy ratio and (c) sensible enthalpy of LHTES system for four-tube eccentric case

5.5. Four Tubes In A Rectangular Shell

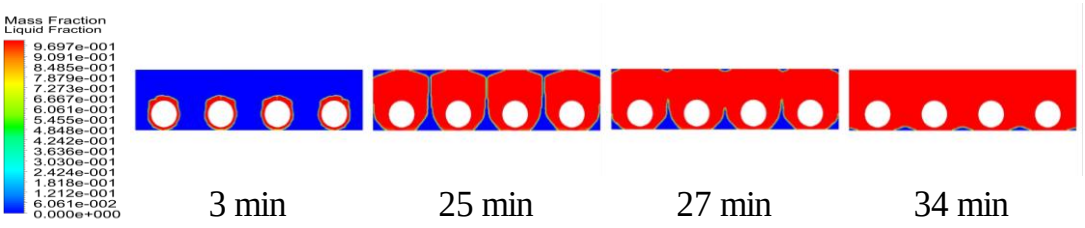

Figure 5.10. Evolution of liquid fraction contours for four-tube with rectangular shell

Here, we pack the melted regions into the fixed space as discussed in two tube case. However, in order to have a manufacturable design we decided the shell to be rectangular. Likewise, in previous sections, the volume of the PCM and tubes are fixed. Inner tubes are 23.9 mm away and the side tubes located 11.95 mm further from the vertical wall of the shell. The length scales of the shell is $175.6\text{mm} \times 44.72\text{mm}$. The previous cases documented that the region below the tubes melts slowly due to dominant heat transfer mechanism is conduction. Therefore, the distance between bottom edge of the shell and the inner tubes reduced to 2 mm.

Figure 5.10 shows how the melting occurs in four tube case with rectangular shell relative to the time. At the 3rd minute, melted region below the tube touches to the shell and begins to expand in horizontal direction. By the 25th minute, the melted regions merge. 81% of PCM melted at the 27th minute, and the rest required 8 more additional minutes as can be seen in Figs. 5.11a and 5.1b. This result shows the rectangular shell design is superior to the previous ones. In addition, Figure 5.11c confirms that the sensible heat begins to increase rapidly as the melted regions touch and their top intersect with the top of the shell.

In order to compare the effect of position of inner tubes and shell design, the results of four tubes compared in Fig. 5.12. Figure 5.12a shows that melting time decreases and S-curve melting becomes steeper as the tubes located in eccentric fashion and even more with rectangular shell shape. Please note that the S-curve of melting is the same until the melted regions intersect for each case, then the trend becomes to change. Fig. 5.12b and 5.12c show that sensible enthalpy becomes the smallest with the

rectangular shell design even the stored latent energy is the greatest. This shows that packing melted regions into a shell is a valid approach which is also easier to conduct.

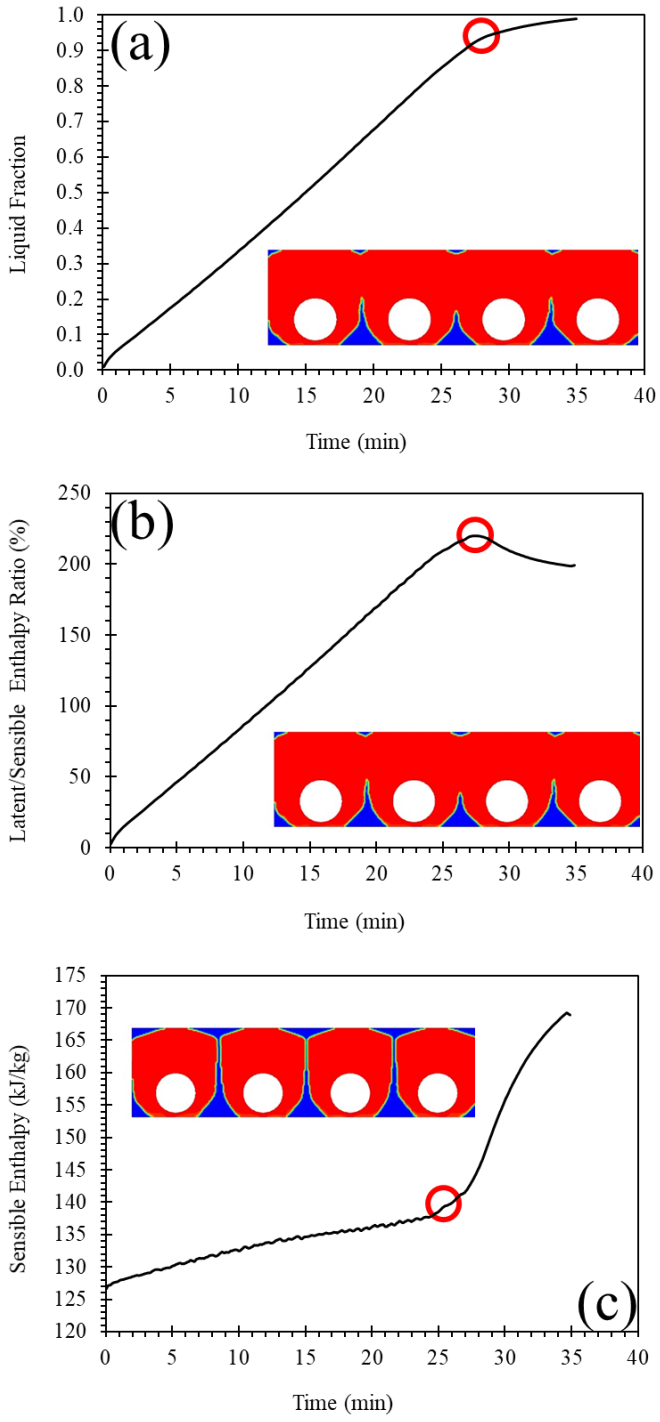

Figure 5.11. Transient variation of (a) liquid fraction, (b) latent/sensible enthalpy ratio and (c) sensible enthalpy of LHTES system for four-tube with rectangular shell

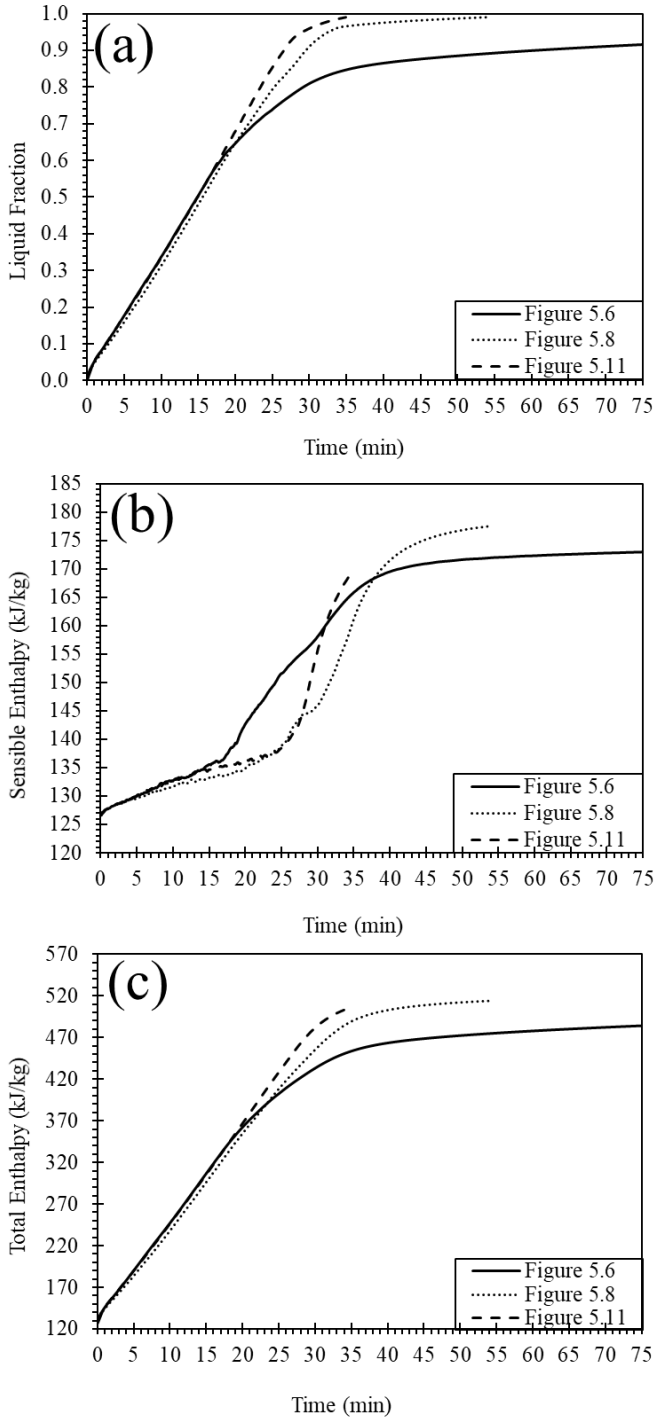

Figure 5.12. Comparison of four-tube cases in terms of (a) liquid fraction, (b) sensible enthalpy and (c) total enthalpy

The figures also show that eccentric tube design yields increase in both sensible and total required energy to melt PCM entirely in comparison to the concentric one, i.e. 1.1% and 0.7% increase in sensible and total enthalpies, respectively. This relatively

small increase can be explained with the enhanced natural convection in between the region near the tubes. Thermal conductance increases due to the length scale of the melted region increases. Overall, Fig. 5.12 documents that the tubes placed in a rectangular shell yields decrease in melting time and required sensible energy.

CHAPTER 6

CONCLUSION

The thesis documents how HTF tubes should be located and what should be the shape of shell tube to enhance melting time of PCM and decrease the required sensible enthalpy for the process. First, a base design which has two tubes located in a circular shell was simulated. The results are in agreement with the literature, and they show that melting below the tubes require most of the melting time and increases sensible enthalpy requirement greatly. Therefore, it is decided to pack melted regions in order to decrease melting time. Note that the volumes of PCM and tubes are fixed; therefore, material originally located below the tubes placed around the tubes. The improved design is selected to be rectangular due to simplicity to manufacture. Results show melting time decreases 52% from concentric design to rectangular design. Then, effect of tube location and shell design was uncovered for four tubes. Results show that in order to minimize both melting time and sensible heat tubes should be located near the bottom end of the shell and the shell should be rectangular. Overall, the study shows melting time and sensible heat can be decreased by just altering the design of the shell and positions of the tubes. In addition, the optimal locations of tubes and shell shape can be decided with packing melted regions around the tubes which does not require exhaustive search.

The current work focused on the effect of shell shape and HTF tube location during the melting process. There are still some challenges to material science. PCMs in use need improvements on the thermophysical properties, especially supercooling and thermal stability. Moreover, enhancement methods like eccentric arrangements in natural convection heat transfer affect the melting process positively, but these approaches are not beneficial for the solidification. To obtain an efficient LHTES unit for both charging and discharging processes, TCE methods such as using fins or nanoparticles can be recommended for future works as long as the methods are being congruent with natural convection progress of the melting process.

REFERENCES

"(No Title)." n.d. Accessed June 3, 2020. http://www.eurosolar.org/new/pdfs_neu/Thermal/IRES2006_Dieckmann.pdf.

"1973 Oil Crisis - Wikipedia." n.d. Accessed May 24, 2020. https://en.wikipedia.org/wiki/1973_oil_crisis.

Achkari, O., and A. El Fadar. 2020. "Latest Developments on TES and CSP Technologies – Energy and Environmental Issues, Applications and Research Trends." *Applied Thermal Engineering* 167 (December 2019): 114806. https://doi.org/10.1016/j.applthermaleng.2019.114806.

Adinberg, R, D Zvegilsky, and M Epstein. 2009. "Heat Transfer Efficient Thermal Energy Storage for Steam Generation." https://doi.org/10.1016/j.enconman.2009.08.006.

Agyenim, Francis. 2016. "The Use of Enhanced Heat Transfer Phase Change Materials (PCM) to Improve the Coefficient of Performance (COP) of Solar Powered LiBr/H2O Absorption Cooling Systems." *Renewable Energy* 87: 229–39. https://doi.org/10.1016/j.renene.2015.10.012.

Agyenim, Francis, Philip Eames, and Mervyn Smyth. 2010. "Heat Transfer Enhancement in Medium Temperature Thermal Energy Storage System Using a Multitube Heat Transfer Array." *Renewable Energy* 35 (1): 198–207. https://doi.org/10.1016/j.renene.2009.03.010.

Al-Abidi, Abduljalil A., Sohif Bin Mat, K. Sopian, M. Y. Sulaiman, and Abdulrahman Th Mohammed. 2013. "CFD Applications for Latent Heat Thermal Energy Storage: A Review." *Renewable and Sustainable Energy Reviews* 20: 353–63. https://doi.org/10.1016/j.rser.2012.11.079.

"Analysis: Coronavirus Temporarily Reduced China's CO2 Emissions by a Quarter." n.d. Accessed May 25, 2020. https://www.carbonbrief.org/analysis-coronavirus-has-temporarily-reduced-chinas-co2-emissions-by-a-quarter?utm_content=bufferae67b&utm_medium=social&utm_source=twitter.com

&utm_campaign=buffer.

"ANSYS Fluent Software | CFD Simulation." 2019. ANSYS, Inc. 2019. https://www.ansys.com/products/fluids/ansys-fluent.

Barrio, E. Palomo del, A. Godin, M. Duquesne, J. Daranlot, J. Jolly, W. Alshaer, T. Kouadio, and A. Sommier. 2017. "Characterization of Different Sugar Alcohols as Phase Change Materials for Thermal Energy Storage Applications." *Solar Energy Materials and Solar Cells* 159 (September 2016): 560–69. https://doi.org/10.1016/j.solmat.2016.10.009.

Bhagat, Kunal, Mohit Prabhakar, and Sandip K. Saha. 2018. "Estimation of Thermal Performance and Design Optimization of Finned Multitube Latent Heat Thermal Energy Storage." *Journal of Energy Storage* 19 (July): 135–44. https://doi.org/10.1016/j.est.2018.06.014.

Brent, A. D., V. R. Voller, and K. J. Reid. 1988. "Enthalpy-Porosity Technique for Modeling Convection-Diffusion Phase Change: Application to the Melting of a Pure Metal." *Numerical Heat Transfer* 13 (3): 297–318. https://doi.org/10.1080/10407788808913615.

Cao, Xiaoling, Yanping Yuan, Bo Xiang, and Fariborz Highlight. 2018. "Effect of Natural Convection on Melting Performance of Eccentric Horizontal Shell and Tube Latent Heat Storage Unit." *Sustainable Cities and Society* 38 (September 2017): 571–81. https://doi.org/10.1016/j.scs.2018.01.025.

Cao, Xiaoling, Yanping Yuan, Bo Xiang, Liangliang Sun, and Zhang Xingxing. 2018. "Numerical Investigation on Optimal Number of Longitudinal Fins in Horizontal Annular Phase Change Unit at Different Wall Temperatures." *Energy and Buildings*. https://doi.org/10.1016/j.enbuild.2017.10.029.

Carrasco Portaspana, Jennifer. 2011. "High Temperature Thermal Energy Storage Systems Based on Latent and Thermo-Chemical Heat Storage," no. 1029166: 81.

Celik, Acar, Hüseyin Coban, Sinan Göcmen, Mehmet Akif Ezan, Aytac Gören, and Aytunc Erek. 2019. "Passive Thermal Management of the Lithium-Ion Battery Unit for a Solar Racing Car." *International Journal of Energy Research* 43 (8):

3681–91. https://doi.org/10.1002/er.4521.

Cetkin, E., S. Lorente, and A. Bejan. 2012. “The Steepest S Curve of Spreading and Collecting Flows: Discovering the Invading Tree, Not Assuming It.” *Journal of Applied Physics* 111 (11). https://doi.org/10.1063/1.4721657.

Coccia, Gianluca, Alessia Aquilanti, Sebastiano Tomassetti, Gabriele Comodi, and Giovanni Di Nicola. 2020. “Design, Realization, and Tests of a Portable Solar Box Cooker Coupled with an Erythritol-Based PCM Thermal Energy Storage.” *Solar Energy* 201 (May): 530–40. https://doi.org/10.1016/j.solener.2020.03.031.

D Laing, T Bauer, W.D Steinmann, D Lehamann. 2009. “Advanced High Temperature Latent Heat Storage System- Design and Test Results.” *Advanced High Temperature Latent Heat Storage System- Design and Test Results*, no. June: 1–8.

Dandotiya, Devendra, and N. D. Banker. 2017. “Numerical Investigation of Heat Transfer Enhancement in a Multitube Thermal Energy Storage Heat Exchanger Using Fins.” *Numerical Heat Transfer; Part A: Applications* 72 (5): 389–400. https://doi.org/10.1080/10407782.2017.1376976.

Darzi, Ahmad Ali Rabienataj, Mousa Farhadi, and Kurosh Sedighi. 2012. “Numerical Study of Melting inside Concentric and Eccentric Horizontal Annulus.” *Applied Mathematical Modelling* 36 (9): 4080–86. https://doi.org/10.1016/j.apm.2011.11.033.

Deng, Shengxiang, Changda Nie, Haojie Jiang, and Wei Biao Ye. 2019. “Evaluation and Optimization of Thermal Performance for a Finned Double Tube Latent Heat Thermal Energy Storage.” *International Journal of Heat and Mass Transfer* 130: 532–44. https://doi.org/10.1016/j.ijheatmasstransfer.2018.10.126.

Deng, Shengxiang, Changda Nie, Guangya Wei, and Wei Biao Ye. 2019. “Improving the Melting Performance of a Horizontal Shell-Tube Latent-Heat Thermal Energy Storage Unit Using Local Enhanced Finned Tube.” *Energy and Buildings* 183: 161–73. https://doi.org/10.1016/j.enbuild.2018.11.018.

Dhaidan, Nabeel S., J. M. Khodadadi, Tahseen A. Al-Hattab, and Saad M. Al-Mashat. 2013. “Experimental and Numerical Investigation of Melting of NePCM inside an

Annular Container under a Constant Heat Flux Including the Effect of Eccentricity." *International Journal of Heat and Mass Transfer* 67: 455–68. https://doi.org/10.1016/j.ijheatmasstransfer.2013.08.002.

Dutta, Ritabrata, Arnab Atta, and Tapas Kumar Dutta. 2008. "Experimental and Numerical Study of Heat Transfer in Horizontal Concentric Annulus Containing Phase Change Material." *Canadian Journal of Chemical Engineering* 86 (4): 700–710. https://doi.org/10.1002/cjce.20075.

Esapour, M., M. J. Hosseini, A. A. Ranjbar, Y. Pahamli, and R. Bahrampoury. 2016. "Phase Change in Multi-Tube Heat Exchangers." *Renewable Energy* 85: 1017–25. https://doi.org/10.1016/j.renene.2015.07.063.

Esapour, Mehdi, Arash Hamzehnezhad, A. Ali Rabienataj Darzi, and Mahmoud Jourabian. 2018. "Melting and Solidification of PCM Embedded in Porous Metal Foam in Horizontal Multi-Tube Heat Storage System." *Energy Conversion and Management* 171 (May): 398–410. https://doi.org/10.1016/j.enconman.2018.05.086.

Ezan, Mehmet Akif, Muhammet Ozdogan, and Aytunç Erek. 2011. "Experimental Study on Charging and Discharging Periods of Water in a Latent Heat Storage Unit." *International Journal of Thermal Sciences* 50 (11): 2205–19. https://doi.org/10.1016/j.ijthermalsci.2011.06.010.

Faghani, M., M. J. Hosseini, and R. Bahrampoury. 2018. "Numerical Simulation of Melting between Two Elliptical Cylinders." *Alexandria Engineering Journal* 57 (2): 577–86. https://doi.org/10.1016/j.aej.2017.02.003.

Gau, C., and R. Viskanta. 1986. "Melting and Solidification of a Pure Metal on a Vertical Wall." *Journal of Heat Transfer* 108 (1): 174–81. https://doi.org/10.1115/1.3246884.

Gorzin, Majid, Mohammad J. Hosseini, Ali A. Ranjbar, and Rasool Bahrampoury. 2018. "Investigation of PCM Charging for the Energy Saving of Domestic Hot Water System." *Applied Thermal Engineering* 137 (April): 659–68. https://doi.org/10.1016/j.applthermaleng.2018.04.016.

"Heat – Renewables 2019 – Analysis - IEA." n.d. Accessed May 26, 2020. https://www.iea.org/reports/renewables-2019/heat#abstract.

Hosseini, M. J., A. A. Ranjbar, M. Rahimi, and R. Bahrampoury. 2015. "Experimental and Numerical Evaluation of Longitudinally Finned Latent Heat Thermal Storage Systems." *Energy and Buildings*. https://doi.org/10.1016/j.enbuild.2015.04.045.

IEA. 2019. "World Energy Outlook 2019 エグゼクティブサマリー." https://webstore.iea.org/download/summary/2467?fileName=Japanese-Summary-WEO2019.pdf.

———. 2020. "Global Energy Review 2020." *Iea*, no. April. https://www.iea.org/reports/global-energy-review-2020.

IRENA International Renewable Energy Agency. 2018. *Renewable Power Generation Costs in 2017*. *International Renewable Energy Agency*. https://doi.org/10.1007/SpringerReference_7300.

Ji, Chenzhen, Zhen Qin, Zhenghua Low, Swapnil Dubey, Fook Hoong Choo, and Fei Duan. 2018. "Non-Uniform Heat Transfer Suppression to Enhance PCM Melting by Angled Fins." *Applied Thermal Engineering* 129: 269–79. https://doi.org/10.1016/j.applthermaleng.2017.10.030.

Jourabian, Mahmoud, Mousa Farhadi, and Ahmad Ali Rabienataj Darzi. 2017. "Accelerated Melting of PCM in a Multitube Annulus-Type Thermal Storage Unit Using Lattice Boltzmann Simulation." *Heat Transfer - Asian Research* 46 (8): 1499–1525. https://doi.org/10.1002/htj.21286.

Jourabian, Mahmoud, Mousa Farhadi, Ahmad Ali Rabienataj Darzi, and Abbas Abouei. 2013. "Lattice Boltzmann Simulation of Melting Phenomenon with Natural Convection from an Eccentric Annulus." *Thermal Science* 17 (3): 877–90. https://doi.org/10.2298/TSCI110510012J.

Joybari, Mahmood Mastani, Fariborz Haghighat, Saeid Seddegh, and Abduljalil A. Al-Abidi. 2017. "Heat Transfer Enhancement of Phase Change Materials by Fins under Simultaneous Charging and Discharging." *Energy Conversion and Management* 152 (April): 136–56.

https://doi.org/10.1016/j.enconman.2017.09.018.

Junior, J. F.Raymundo, R. De Cesaro Oliveski, L. A.O. Rocha, and C. Biserni. 2018. "Numerical Investigation on Phase Change Materials (PCM): The Melting Process of Erythritol in Spheres under Different Thermal Conditions." *International Journal of Mechanical Sciences* 148 (August): 20–30. https://doi.org/10.1016/j.ijmecsci.2018.08.006.

Kalapala, Lokesh, and Jaya Krishna Devanuri. 2018. "Influence of Operational and Design Parameters on the Performance of a PCM Based Heat Exchanger for Thermal Energy Storage – A Review." *Journal of Energy Storage* 20 (September): 497–519. https://doi.org/10.1016/j.est.2018.10.024.

Kato, Yukitaka, Rui Takahashi, Toshiya Sekiguchi, and Junichi Ryu. 2009. "Study on Medium-Temperature Chemical Heat Storage Using Mixed Hydroxides." *International Journal of Refrigeration* 32 (4): 661–66. https://doi.org/10.1016/j.ijrefrig.2009.01.032.

Kazemi, M., M. J. Hosseini, A. A. Ranjbar, and R. Bahrampoury. 2018. "Improvement of Longitudinal Fins Configuration in Latent Heat Storage Systems." *Renewable Energy* 116: 447–57. https://doi.org/10.1016/j.renene.2017.10.006.

Kenisarin, Murat M. 2010. "High-Temperature Phase Change Materials for Thermal Energy Storage." *Renewable and Sustainable Energy Reviews* 14 (3): 955–70. https://doi.org/10.1016/j.rser.2009.11.011.

Kousha, N., M. Rahimi, R. Pakrouh, and R. Bahrampoury. 2019. "Experimental Investigation of Phase Change in a Multitube Heat Exchanger." *Journal of Energy Storage* 23 (March): 292–304. https://doi.org/10.1016/j.est.2019.03.024.

Kurnia, Jundika C., and Agus P. Sasmito. 2018. "Numerical Investigation of Heat Transfer Performance of a Rotating Latent Heat Thermal Energy Storage." *Applied Energy* 227 (January): 542–54. https://doi.org/10.1016/j.apenergy.2017.08.087.

Laing, Doerte, Carsten Bahl, Thomas Bauer, Dorothea Lehmann, and Wolf Dieter Steinmann. 2011a. "Thermal Energy Storage for Direct Steam Generation." *Solar Energy*. https://doi.org/10.1016/j.solener.2010.08.015.

———. 2011b. “Thermal Energy Storage for Direct Steam Generation.” *Solar Energy* 85 (4): 627–33. https://doi.org/10.1016/j.solener.2010.08.015.

Lakhani, Sagar, Appasaheb Raul, and Sandip K. Saha. 2017. “Dynamic Modelling of ORC-Based Solar Thermal Power Plant Integrated with Multitube Shell and Tube Latent Heat Thermal Storage System.” *Applied Thermal Engineering* 123: 458–70. https://doi.org/10.1016/j.applthermaleng.2017.05.115.

“Lazard.Com | Levelized Cost of Energy and Levelized Cost of Storage 2018.” n.d. Accessed January 20, 2020. https://www.lazard.com/perspective/levelized-cost-of-energy-and-levelized-cost-of-storage-2018/.

Liu, Chang, and Dominic Groulx. 2014. “Experimental Study of the Phase Change Heat Transfer inside a Horizontal Cylindrical Latent Heat Energy Storage System.” *International Journal of Thermal Sciences* 82 (1): 100–110. https://doi.org/10.1016/j.ijthermalsci.2014.03.014.

Liu, Zhenyu, Yuanpeng Yao, and Huiying Wu. 2013. “Numerical Modeling for Solid-Liquid Phase Change Phenomena in Porous Media: Shell-and-Tube Type Latent Heat Thermal Energy Storage.” *Applied Energy* 112: 1222–32. https://doi.org/10.1016/j.apenergy.2013.02.022.

Lucia, M. De, and A. Bejan. 1991. “Thermodynamics of Phase-Change Energy Storage: The Effects of Liquid Superheating during Melting, and Irreversibility during Solidification.” *Journal of Solar Energy Engineering, Transactions of the ASME* 113 (1): 2–10. https://doi.org/10.1115/1.2929947.

Luo, Kang, Feng Ju Yao, Hong Liang Yi, and He Ping Tan. 2015. “Lattice Boltzmann Simulation of Convection Melting in Complex Heat Storage Systems Filled with Phase Change Materials.” *Applied Thermal Engineering* 86: 238–50. https://doi.org/10.1016/j.applthermaleng.2015.04.059.

Mat, Sohif, Abduljalil A. Al-Abidi, K. Sopian, M. Y. Sulaiman, and Abdulrahman Th Mohammad. 2013. “Enhance Heat Transfer for PCM Melting in Triplex Tube with Internal-External Fins.” *Energy Conversion and Management*. https://doi.org/10.1016/j.enconman.2013.05.003.

Nazzi Ehms, J. H., R. De Césaro Oliveski, L. A. Oliveira Rocha, and C. Biserni. 2018. "Theoretical and Numerical Analysis on Phase Change Materials (PCM): A Case Study of the Solidification Process of Erythritol in Spheres." *International Journal of Heat and Mass Transfer* 119: 523–32. https://doi.org/10.1016/j.ijheatmasstransfer.2017.11.124.

Niyas, Hakeem, Sunku Prasad, and P. Muthukumar. 2017. "Performance Investigation of a Lab–Scale Latent Heat Storage Prototype – Numerical Results." *Energy Conversion and Management*. https://doi.org/10.1016/j.enconman.2016.12.075.

Pahamli, Younes, Mohammad J. Hosseini, Ali A. Ranjbar, and Rasool Bahrampoury. 2016. "Analysis of the Effect of Eccentricity and Operational Parameters in PCM-Filled Single-Pass Shell and Tube Heat Exchangers." *Renewable Energy* 97: 344–57. https://doi.org/10.1016/j.renene.2016.05.090.

Parry, Andrew J., Philip C. Eames, and Francis B. Agyenim. 2014. "Modeling of Thermal Energy Storage Shell-and-Tube Heat Exchanger." *Heat Transfer Engineering* 35 (1): 1–14. https://doi.org/10.1080/01457632.2013.810057.

Parsazadeh, Mohammad, and Xili Duan. 2018. "Numerical Study on the Effects of Fins and Nanoparticles in a Shell and Tube Phase Change Thermal Energy Storage Unit." *Applied Energy* 216 (April): 142–56. https://doi.org/10.1016/j.apenergy.2018.02.052.

Pizzolato, Alberto, Ashesh Sharma, Kurt Maute, Adriano Sciacovelli, and Vittorio Verda. 2017. "Design of Effective Fins for Fast PCM Melting and Solidification in Shell-and-Tube Latent Heat Thermal Energy Storage through Topology Optimization." *Applied Energy* 208 (October): 210–27. https://doi.org/10.1016/j.apenergy.2017.10.050.

Qiu, Lin, Yuxin Ouyang, Yanhui Feng, and Xinxin Zhang. 2019. "Review on Micro/Nano Phase Change Materials for Solar Thermal Applications." *Renewable Energy* 140: 513–38. https://doi.org/10.1016/j.renene.2019.03.088.

Rathod, Manish K., and Jyotirmay Banerjee. 2015. "Thermal Performance Enhancement of Shell and Tube Latent Heat Storage Unit Using Longitudinal Fins." *Applied Thermal Engineering* 75: 1084–92.

https://doi.org/10.1016/j.applthermaleng.2014.10.074.

Raul, Appasaheb K., Pratik Bhavsar, and Sandip Kumar Saha. 2018. “Experimental Study on Discharging Performance of Vertical Multitube Shell and Tube Latent Heat Thermal Energy Storage.” *Journal of Energy Storage* 20 (September): 279–88. https://doi.org/10.1016/j.est.2018.09.022.

Ritchie, Hannah, and Max Roser. 2018. “Urbanization - Our World in Data.” *Our World in Data*. https://ourworldindata.org/urbanization#citation.

Rozenfeld, T., Y. Kozak, R. Hayat, and G. Ziskind. 2015. “Close-Contact Melting in a Horizontal Cylindrical Enclosure with Longitudinal Plate Fins: Demonstration, Modeling and Application to Thermal Storage.” *International Journal of Heat and Mass Transfer* 86: 465–77. https://doi.org/10.1016/j.ijheatmasstransfer.2015.02.064.

Sciacovelli, A., F. Gagliardi, and V. Verda. 2015. “Maximization of Performance of a PCM Latent Heat Storage System with Innovative Fins.” *Applied Energy* 137: 707–15. https://doi.org/10.1016/j.apenergy.2014.07.015.

Seddegh, Saeid, Xiaolin Wang, and Alan D. Henderson. 2016. “A Comparative Study of Thermal Behaviour of a Horizontal and Vertical Shell-and-Tube Energy Storage Using Phase Change Materials.” *Applied Thermal Engineering* 93: 348–58. https://doi.org/10.1016/j.applthermaleng.2015.09.107.

Shinde, Asmita, Sankalp Arpit, Pramod Km, Peddy V.C. Rao, and Sandip K. Saha. 2017. “Heat Transfer Characterization and Optimization of Latent Heat Thermal Storage System Using Fins for Medium Temperature Solar Applications.” *Journal of Solar Energy Engineering, Transactions of the ASME* 139 (3). https://doi.org/10.1115/1.4035517.

Steinmann, Wolf Dieter, and Rainer Tamme. 2008. “Latent Heat Storage for Solar Steam Systems.” In *Journal of Solar Energy Engineering, Transactions of the ASME*, 130:0110041–45. https://doi.org/10.1115/1.2804624.

Tao, Y. B., and Y. L. He. 2015. “Effects of Natural Convection on Latent Heat Storage Performance of Salt in a Horizontal Concentric Tube.” *Applied Energy* 143: 38–46.

https://doi.org/10.1016/j.apenergy.2015.01.008.

Vaivudh, Sarayooth, Wattanapong Rakwichian, and Sirinuch Chindaruksa. 2008. “Heat Transfer of High Thermal Energy Storage with Heat Exchanger for Solar Trough Power Plant.” *Energy Conversion and Management* 49 (11): 3311–17. https://doi.org/10.1016/j.enconman.2008.04.013.

Vogel, J., J. Felbinger, and M. Johnson. 2016. “Natural Convection in High Temperature Flat Plate Latent Heat Thermal Energy Storage Systems.” *Applied Energy* 184: 184–96. https://doi.org/10.1016/j.apenergy.2016.10.001.

Vogel, J., and M. Johnson. 2019. “Natural Convection during Melting in Vertical Finned Tube Latent Thermal Energy Storage Systems.” *Applied Energy* 246 (December 2018): 38–52. https://doi.org/10.1016/j.apenergy.2019.04.011.

Wang, Peilun, Hua Yao, Zhipeng Lan, Zhijian Peng, Yun Huang, and Yulong Ding. 2016. “Numerical Investigation of PCM Melting Process in Sleeve Tube with Internal Fins.” *Energy Conversion and Management* 110: 428–35. https://doi.org/10.1016/j.enconman.2015.12.042.

Wang, Yifei, Liang Wang, Ningning Xie, Xipeng Lin, and Haisheng Chen. 2016. “Experimental Study on the Melting and Solidification Behavior of Erythritol in a Vertical Shell-and-Tube Latent Heat Thermal Storage Unit.” *International Journal of Heat and Mass Transfer* 99: 770–81. https://doi.org/10.1016/j.ijheatmasstransfer.2016.03.125.

Wolff, F., and R. Viskanta. 1987. “Melting of a Pure Metal from a Vertical Wall.” *Experimental Heat Transfer* 1 (1): 17–30. https://doi.org/10.1080/08916158708946328.

Yusuf Yazici, M., Mete Avci, Orhan Aydin, and Mithat Akgun. 2014. “Effect of Eccentricity on Melting Behavior of Paraffin in a Horizontal Tube-in-Shell Storage Unit: An Experimental Study.” *Solar Energy* 101: 291–98. https://doi.org/10.1016/j.solener.2014.01.007.

Zeng, Ju Lan, Lei Zhou, Yue Fei Zhang, Sai Ling Sun, Yu Hang Chen, Li Shu, Lin Ping Yu, Ling Zhu, Liu Bin Song, and Zhong Cao. 2017. “Effects of Some Nucleating

Agents on the Supercooling of Erythritol to Be Applied as Phase Change Material." *Journal of Thermal Analysis and Calorimetry* 129 (3): 1291–99. https://doi.org/10.1007/s10973-017-6296-2.

Zhang, Nan, and Yanxia Du. 2018. "Ultrasonic Enhancement on Heat Transfer of Palmitic-Stearic Acid as PCM in Unit by Experimental Study." *Sustainable Cities and Society* 43 (September): 532–37. https://doi.org/10.1016/j.scs.2018.08.040.

Zhao, C. Y., and Z. G. Wu. 2011. "Heat Transfer Enhancement of High Temperature Thermal Energy Storage Using Metal Foams and Expanded Graphite." *Solar Energy Materials and Solar Cells* 95 (2): 636–43. https://doi.org/10.1016/j.solmat.2010.09.032.

Zheng, Zhang Jing, Yang Xu, and Ming Jia Li. 2018. "Eccentricity Optimization of a Horizontal Shell-and-Tube Latent-Heat Thermal Energy Storage Unit Based on Melting and Melting-Solidifying Performance." *Applied Energy* 220 (March): 447–54. https://doi.org/10.1016/j.apenergy.2018.03.126.